

Investigation of Additively Manufactured AlSi12 Kelvin Lattice Structures

Olzhas Raimbekov, B.Eng.

**Submitted in fulfillment of the requirements
for the degree of Master of Science
in Mechanical & Aerospace Engineering**



**NAZARBAYEV
UNIVERSITY**

**School of Engineering and Digital Sciences
Department of Mechanical & Aerospace Engineering
Nazarbayev University**

53 Kabanbay Batyr Avenue,
Astana, Kazakhstan, 010000

Supervisor: Associate Professor Didier Talamona
Co-supervisor: Associate Professor Asma Perveen

April 2024

DECLARATION

I hereby, declare that this manuscript, entitled “*Investigation of Additively Manufactured AlSi12 Kelvin Lattice Structures*”, is the result of my own work except for quotations and citations, which have been duly acknowledged.

I also declare that, to the best of my knowledge and belief, it has not been previously or concurrently submitted, in whole or in part, for any other degree or diploma at Nazarbayev University or any other national or intentional institution.



Name: Olzhas Raimbekov

Date: 08.04.2024

Abstract

Additive Manufacturing (AM) has facilitated the production of parts with complex geometries. A particularly notable application of AM lies in the development of structured materials or lattice structures, where the mechanical attributes are dictated more by shape and design than by the material's microstructure itself. Lattice structures are crafted by designing the unit cell's topology in every direction of space. This in turn offers lightweight and customizable mechanical characteristics for applications in aerospace, biomedical, and automotive fields. Although research has been conducted on lattice structures made from materials such as Ti, AlSi12Mg, and Fe alloys, studies on lattices composed of AlSi12 alloys are somewhat limited. However, given their lower density compared to steel, AlSi12 alloys represent a potentially more economical alternative to Ti-based alloys. Despite this advantage, the production of lattice structures from AlSi12 alloys has not become widespread. This study is devoted to the mechanical properties of compression of lattice structures of AlSi12 alloy. It describes how these properties and energy absorption capabilities are affected by structure geometry, evaluates the impact of different thermal treatments on performance, and explores new lattice configurations with improved performance by combining Kelvin lattice and BCC lattice. A study was carried out on kelvin lattices with different strut diameters and unit cell sizes to evaluate their mechanical properties and energy absorption capacity. It has been found that non heat treated lattices have a significantly higher energy absorption capacity than those that have been heat treated. Among them, the as-built kelvin lattice combined with the BCC configuration showed the maximum energy absorption capacity measured at 416 MJ/m^3 . In contrast, a heat-treated kelvin lattice with a unit cell size of 6 mm demonstrated a minimum capacitance of 9 MJ/m^3 . The as-built lattice exhibits superior mechanical characteristics but demonstrates considerable brittleness. This results in the formation of a shear band during compression, leading to a separative failure of lattice. This problem is directly related to the microstructural composition of the alloy, which includes a fibrous network of silicon surrounding a delicate Al phase. In addition, it has been observed that heat treatment negatively affects the energy absorption ability of the lattices. The effect of heat treatment varies depending on various mechanical aspects such as yield stress, Young's modulus and plateau stress. Notably, heat treatment changes the stress-strain behavior from a stretch dominated response to a bending dominated response.

Through microstructural research, it was observed that heat treatment leads to the formation of Si agglomerates, which increase the ductility of the lattices.

Table of Contents

Abstract.....	2
List of Abbreviations & Symbols.....	5
List of Tables.....	6
List of Figures.....	7
Chapter 1 – Introduction.....	9
1.1. Selective laser melting additive manufacturing.....	9
1.2. Overview of lattice structures.....	10
Chapter 2 – Literature Review.....	11
2.1. Characterization of Lattice Structures.....	11
2.2. Investigated Strut Based Lattice Structures.....	13
2.3. Heat Treatment Processes on AlSi12.....	18
2.4. Mechanical properties of lattice structures.....	21
2.5. Research Gap.....	23
2.6. Motivation, Aim and Objectives.....	24
Chapter 3 – Methodology.....	26
3.1. Powder description.....	26
3.2. Lattice structures and tensile specimens.....	28
3.3. SLM process parameters.....	31
3.4. Specimens characterization.....	32
3.5. Heat Treatment.....	33
Chapter 4 - Results and Discussion.....	34
4.1 Tensile test.....	34
4.2 Compression test of non heat treated kelvin lattices.....	35
4.3 Compression test of heat treated kelvin lattices.....	38
4.4 Compression test for hybrid kelvin lattices.....	41
4.5 Deformation patterns of non heat treated lattices.....	44
4.6 Deformation patterns heat treated lattices.....	45
4.7 Tensile specimens fractography.....	46
4.8 Microstructure investigation.....	48
Chapter 5 – Conclusions.....	51
Chapter 6 – Future work.....	52
References.....	53
Acknowledgements.....	59
Appendices.....	60

List of Abbreviations & Symbols

AM	Additive Manufacturing
EDS	Energy Dispersive Spectroscopy
PBF	Powder Bed Fusion
SEM	Scanning Electron Microscope
SLM	Selective Laser Melting
UTS	Ultimate Tensile Strength
σ	Stress
F	Load
A0	Cross-Section Area
ε	Strain
Δh	Change in Height
h0	Initial Height
ψ	Energy Absorption
σ_p	Plateau Stress

List of Tables

TABLE 2.2.1: TABULAR SUMMARY OF VARIOUS INVESTIGATED LATTICE STRUCTURES	16
TABLE 3.1.1: TABULAR SUMMARY OF POWDER CHEMICAL COMPOSITION	25
TABLE 3.2.1: LATTICE STRUCTURES' CHARACTERISTICS	28
TABLE 3.3.1. PRINTING PARAMETERS	30

List of Figures

Figure 1.1.1: Operating principle of SLM 3D printer.....	9
Figure 2.1.1: Cellular structures across various topologies utilize unit cells as their fundamental building blocks. These include: a) cellular structures based on struts, b) cellular configurations utilizing skeletal triply periodic minimal surfaces, and c) cellular designs that employ sheet-like triply periodic minimal surfaces configurations [30].....	13
Figure 2.4.1: 2D schematic of bending (a) and stretch dominated (b) deformations.....	23
Figure 2.4.2: Standard stress-strain diagrams stretching dominated and bending dominated structures under uniaxial compression [61].....	24
Figure 2.4.3: Schematic of mechanical properties of lattice structures [62].....	24
Figure 3.1.1: Size distribution of AlSi12 powder.....	28
Figure 3.1.2: AlSi12 morphology at 100 magnification.....	29
Figure 3.1.3: AlSi12 morphology at 550 magnification.....	29
Figure 3.2.1: a) kelvin lattice; b) BCC lattice.....	30
Figure 3.2.2: BCC lattice geometry: a) BCC lattice; b) BCC without kelvin lattice.....	31
Figure 3.2.3: BCC-ALT lattice geometry: a) BCC- ALT lattice; b) BCC-ALT without kelvin lattice.....	31
Figure 3.2.4: Cross-sectional view of Kelvin lattice.....	32
Figure 3.2.5: BCC geometry that was used in hybrid Kelvin lattice: left) Kelvin lattice with BCC; right) Kelvin lattice with altered BCC.....	32
Figure 3.5.1: Heat treatment: temp. vs. time graph.....	34
Figure 4.1.1: Tensile specimens.....	35
Figure 4.1.2: Stress vs. Strain of tensile test for bulk material.....	36
Figure 4.1.3: Mechanical properties of tensile specimens.....	36
Figure 4.2.1: Compressive stress-strain curve of kelvin lattices.....	38
Figure 4.2.2: Compressive mechanical properties of kelvin lattices.....	38
Figure 4.2.3: Energy absorption capacity of kelvin lattices.....	39
Figure 4.3.1: Compressive stress-strain curve of heat treated kelvin lattices.....	40
Figure 4.3.2: Compressive mechanical properties of heat treated kelvin lattices.....	41
Figure 4.3.3: Energy absorption capacity of heat treated kelvin lattices.....	41
Figure 4.4.1: Compressive stress-strain curve of hybrid kelvin lattices.....	42
Figure 4.4.2: Compressive stress-strain curve of heat treated hybrid kelvin lattices.....	43
Figure 4.4.3: Compressive mechanical properties of hybrid kelvin lattices.....	44
Figure 4.4.4: Energy absorption capacity of hybrid kelvin lattices.....	44
Figure 4.5.1: 15 mm Kelvin lattice deformation patterns. a) Initial state of the lattice; b) sinister diagonal (from upper right to lower left) failure moment; c) sinister diagonal complete failure; d) dexter diagonal (from upper left to lower right) failure moment.....	45
Figure 4.5.2: 25 mm Kelvin lattice deformation patterns. a) Initial state of the lattice; b) sinister diagonal (from upper right to lower left) failure moment; c) sinister diagonal	

complete failure; d) dexter diagonal (from upper left to lower right) failure moment.....	46
Figure 4.6.1: Deformation pattern of heat treated kelvin lattice. a) Initial state of the lattice; b) yield point; c) plastic region; d) compression at 0.5 mm/mm strain.....	46
Figure 4.7.1: Tensile specimen fractography.....	47
Figure 4.7.2: Tensile specimen fractography.....	48
Figure 4.7.3: Tensile specimen fractography.....	49
Figure 4.8.1: SEM and EDS images of non heat treated microstructure sample.....	50
Figure 4.8.2: SEM and EDS images of heat treated microstructure sample.....	50
Figure 4.8.3: Microstructure investigation of heat treated sample.....	51
Figure 4.8.4: Microstructure investigation of non heat treated sample.....	51

Chapter 1 – Introduction

1.1. Selective laser melting additive manufacturing

Additive manufacturing (AM) or 3D printing is a rapidly growing technology in the manufacturing industry. This is due to the fact that technology allows the production of structures of any complexity and on various scales: from micrometers to millimeters [1], [2]. The technology also has a wide range of applications and a selection of materials. This opens up the potential for unprecedented design freedom and functional integration [2]. Among AM methodologies, selective laser melting (SLM) stands out as a prominent powder bed fusion (PBF) technology, especially used for layer-by-layer production of metal components.

In the SLM process, desired structures take shape through the precise melting and fusion of metal particles deposited on a powder bed. Subsequent layers are systematically added, perpetuating the iterative progression until the entire 3D geometry is printed. (see Figure 1.1.1).

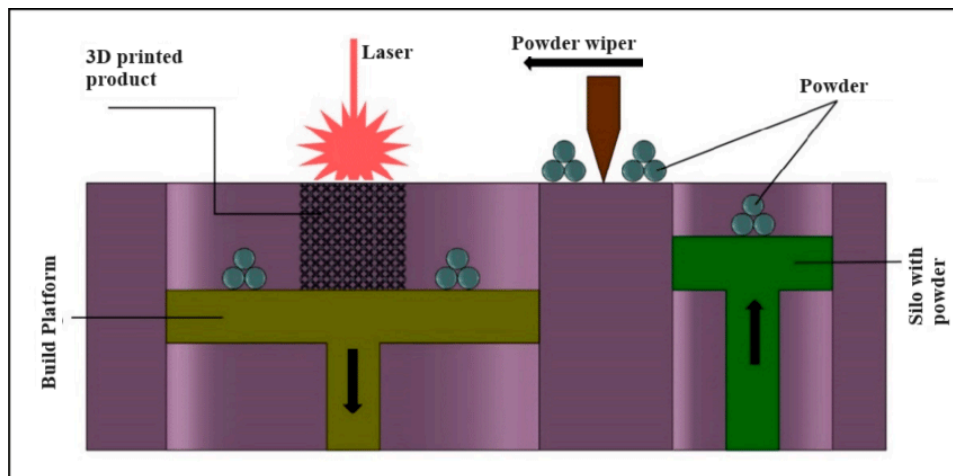


Figure 1.1.1: Operating principle of SLM 3D printer [3]

SLM technology is considered to be versatile due to its ability to create complex geometries and structures that are difficult or impossible to create using traditional manufacturing [2]. The SLM technology opened up ways to create complex lattice structures, optimize topologies more effectively, and generate designs based on highly complex mathematical algorithms [4–13]. At the current level of development, SLM technology continues to develop, and constant research and development is being carried out aimed at expanding its

capabilities and expanding its application. In order to optimize the quality and performance of components produced by SLM, researchers are studying advances in powder materials, laser systems, and process parameters [1]. Improvement of the design process is achieved through the integration of advanced computational tools such as topology optimization and generative design algorithms. This makes it possible to create structures with improved mechanical and functional properties [8-13]. Ultimately, this leads to new opportunities for innovation in materials science and engineering. These opportunities are possible since the study of functionally graded materials in SLM allows the adaptation of material properties within a single component [11-12]. For the aerospace industry, SLM technology opens up new opportunities due to its ability to produce lightweight yet strong components. Such components have a positive effect on the overall efficiency of aerospace vehicles [14]. Interest from various parties involved in the aerospace industry shows that the above-mentioned technology has enormous potential. In addition, ongoing collaboration between researchers, industry experts and regulators addresses challenges associated with standardization and certification, searching the way for greater adoption of SLM in mission-critical applications.

There are several reasons for increasing demand for lightweight structures in the modern technological world. One of the key reasons is to decrease raw material consumption. By adapting production chains of lightweight structures industries utilizing fuel can improve its efficiency, since reducing weight directly correlates with lower fuel consumption. Also, lightweight structures such as lattices often possess high strength-to-weight ratios. These parameters are essential for improving performance of vehicles, as it directly impacts on speed, maximum range, and payload capacity. So, fuel efficiency benefits of lightweight materials contribute to emissions reduction.

1.2. Overview of lattice structures

Lattice structures represent a breakthrough innovation in the pursuit of lightweight design principles, playing a significant role in diverse industries such as aerospace, automotive, medical, and electronics manufacturing [15-18]. The distinctive feature of lattice structures lies in their 3D dimensional ordered open-celled formations, achieved by patterning one or several unit cell

structures in three dimensions. Unlike conventional materials, the strength and stiffness of lattice structures are not dictated by microstructure but rather by the design of the unit cells, enabling unique properties such as low mass, high energy absorption efficiency, negative stiffness, and Poisson ratio.

The customization potential of lattice structures is a key aspect, with properties like porosity and the topology of unit cells being adjustable to meet specific requirements. Due to these exceptional properties, lattice structures have garnered significant attention from both academic and industrial research communities.

Chapter 2 – Literature Review

2.1. Characterization of Lattice Structures

To comprehensively define a lattice structure, it's crucial to fully characterize its unit cell, detailing the structure's design, generation method, and inherent properties. Most existing lattice cells derive from traditional geometrical structures, like the octet truss or the Kagome Lattice, yet the variety is limited (<40), with many being slight variations of others. This raises the need for a clear definition distinguishing 'new' from 'existing' structures to enhance the classification and exploration of lattice designs. Current research lacks a rigorous approach to analyzing how design variables impact structural strength, resulting in a dearth of data for generalizing cell properties. This gap complicates the prediction of a lattice's performance and its optimization in engineering applications. Commercial software for lattice design is limited, offering scant flexibility, a narrow selection of cell types, minimal FEA integration, and restricted optimization capabilities. Lattice structures are generated either manually, using basic geometric forms and requiring extensive post-processing, or mathematically, through algorithms that yield periodic structures without the need for manual adjustment. Despite the predominance of hand-crafted structures due to their simplicity, there is a noticeable gap in methods for approximating such structures to minimize post-processing challenges. Although there is potential for using mathematical patterns to create a variety of lattice structures, there is a lack of guidance in the literature for translating these patterns into practical lattice designs. Each of the existing manual and mathematical generation methods has its own advantages and disadvantages, highlighting the need for further research and development in the design and optimization of lattice structures to fully exploit their unique properties for advanced engineering applications [19].

Lattice structures can be made by two different approaches: stochastic and non-stochastic, each with unique characteristics and applications. Stochastic lattice structures are characterized by chaos and lack of uniformity. This approach takes inspiration from the complex, irregular patterns found in nature, such as the internal structure of bones or the porous nature of wood. The random distribution of nodes and struts in stochastic lattices allows the creation of materials that closely mimic the mechanical and physical properties of natural materials. Such structures are particularly beneficial in applications requiring gradient properties or anisotropy,

such as biomedical implants that need to integrate with bone or lightweight components that require variable stiffness [20-22].

On the other hand, non-stochastic lattice structures are defined by their regular, predictable patterns. This category encompasses several types of lattices, each tailored to specific requirements by altering their geometric configuration. Figure 2.1.1 represents these configurations.

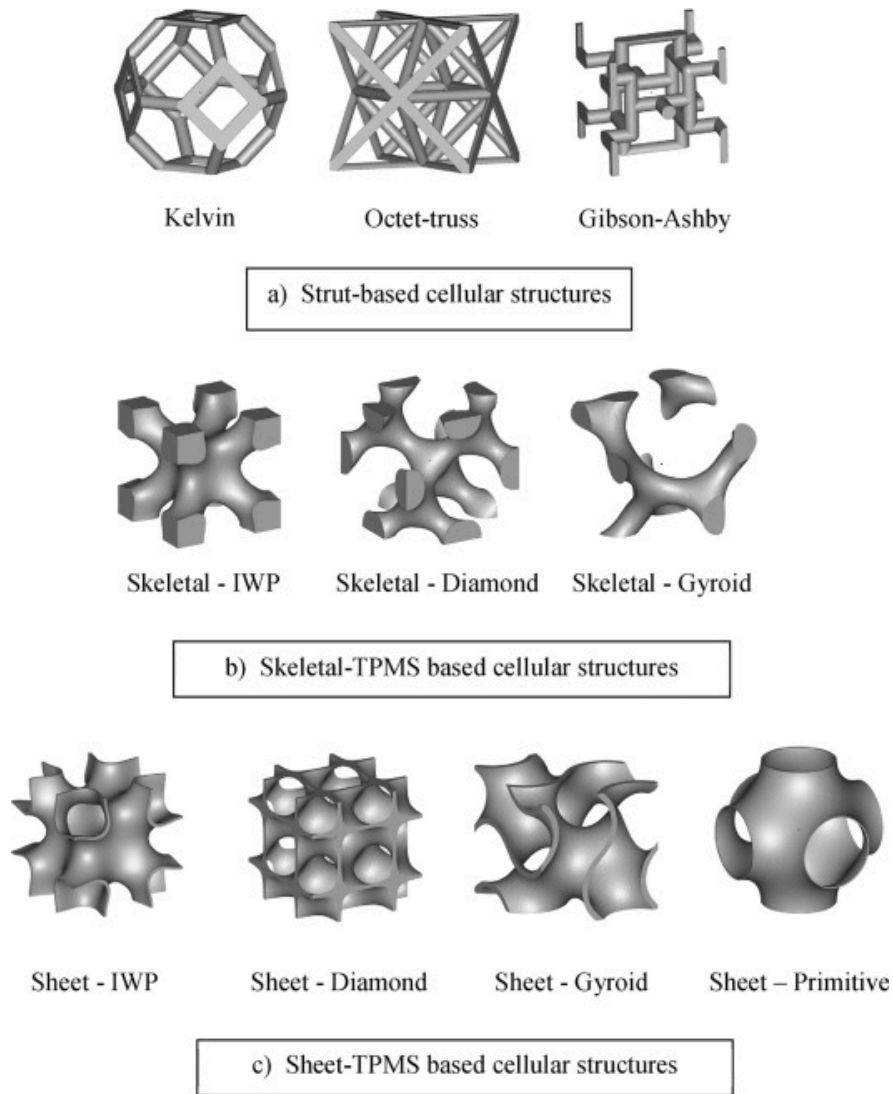


Figure 2.1.1: Cellular structures across various topologies utilize unit cells as their fundamental building blocks. These include: a) cellular structures based on struts, b) cellular configurations utilizing skeletal triply periodic minimal surfaces, and c) cellular designs that employ sheet-like triply periodic minimal surfaces configurations [30]

Strut-Based Lattice Structures are the most straightforward non-stochastic lattices, consisting of straight linear elements connected at nodes. This configuration offers a balance between strength and weight, making it ideal for applications in aerospace and automotive industries where reducing weight without compromising strength is crucial [23-25].

Triple periodic minimal surface (TPMS) lattice structures represent a more sophisticated approach. These structures are based on mathematical surfaces that occur in nature, offering a continuous smooth surface that divides space into two interconnected areas. This unique feature provides isotropic properties, making TPMS lattices suitable for applications requiring uniform strength and stiffness, such as protective equipment and lightweight structural components [26-28].

Skeletal lattice TPMS structures are an option that reduces material consumption by focusing material along the edges of the TPMS geometry. This approach retains the isotropic properties of TPMS lattices but at a significant reduction in weight, making it ideal for applications where material efficiency is paramount without significantly compromising structural integrity [26, 29–31].

Sheet TPMS Lattice Structures thicken the surfaces of TPMS geometries to create robust, sheet-like formations. This modification leads to structures that combine the high surface area and uniform properties of TPMS lattices with enhanced stiffness and strength, suitable for demanding applications in aerospace and automotive sectors where robust yet lightweight materials are essential [27, 32-34].

2.2. Investigated Strut Based Lattice Structures

There are many types of geometry for lattice structures. Overall geometry is characterized by unit cell types. They can be auxetic, face-centered cubic, body-centered cubic, cubic and so on. So, there are investigations that explored the fabrication, characterization, and applications of auxetic materials and structures, primarily focusing on their unique mechanical properties enabled by additive manufacturing technologies. Auxetic materials exhibit a negative Poisson's ratio, expanding laterally when stretched and contracting when compressed, opposite to the behavior of conventional materials. Xue et al. [35] examined the fabrication of Al-based auxetic lattice structures through 3D printing and investment casting technology. Authors

focused on compressive mechanical behavior. As a result, it was identified that the auxetic lattice structures' compression strength and Poisson's ratio depend on the length, diameter, and re-entrant angle of struts. The study suggests that auxetic lattice structures can be enhanced by tailoring these parameters, proposing a new approach to designing materials with desired mechanical properties. Warmuth et al. [36] discuss the development of 3D metallic auxetic metamaterials with tunable mechanical properties, focusing on the influence of design parameters on their behavior. Their research provides insight into parametric studies of auxetic materials to optimize their mechanical properties for various applications. Yuan et al. [37] investigated soft auxetic lattice structures 3D printed by selective laser sintering (SLS). The material used is thermoplastic polyurethane (TPU) powder. It emphasizes a systematic approach to powder evaluation and process optimization for the fabrication of complex 3D structures using TPU. Their research showed that soft metamaterials are capable of maintaining unusual deformations under high loads and withstanding repeated compression cycles. Thus, they concluded that their lattice structure could be used as a mechanical and acoustic energy absorber, actuator, and vibration damper. Schwerdtfeger et al. [38] and Eldesouki et al. [39] investigated the Ti-6Al-4V alloy auxetic structures through mechanical tests. It was fabricated by selective electron beam melting and electron beam melting technologies. Authors concluded that these additive manufacturing methods are able to create well-defined auxetic structures with free-form geometries. This in turn grants high control over mechanical properties such as Young's modulus and Poisson's ratio.

Bai et al. [40] investigate the design of an optimized lattice structure through discrete structure topology optimization. The aim of research is to create a lightweight lattice structure using the ground structure method. To increase mechanical properties of lattice structure they used the firefly algorithm for optimization. The algorithm aims to minimize the volume under force constraints, resulting in a new face-centered cubic (AFCC) structure, which is compared with a traditional body-centered cubic structure for evaluation. Using Ti6Al4V material, an optimized AFCC lattice structure and a reference BCC structure were fabricated using SLM. In order to evaluate mechanical properties both structures underwent quasi-static uniaxial compression testing and finite element analysis. The results showed the superiority of the AFCC structure over the BCC structure in terms of elastic modulus and yield strength, with improvements of 143% and 120%, respectively. In addition, the AFCC structure exhibited

excellent energy absorption capacity, approximately 2.4 times higher compared to the BCC structure at the same degree of deformation.

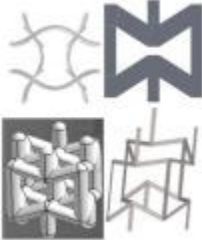

One of the well studied lattice geometry is BCC lattice. For example, Leary et al. [41] investigated the properties of Inconel 625 lattice structures printed by SLM technology. The aim was to create a structure with customized mechanical responses suitable for high temperature applications. Authors mentioned that it is crucial to understand the correlation between printing parameters and the resulting mechanical properties of BCC lattice structures. This understanding will provide a solid foundation for design optimization patterns of lattice structures to achieve high sustainability against physiological loads. Feng et al. [42] presented an analysis of BCC lattice structures made of Ti6Al4V. They established a theoretical approach for predicting mechanical behavior supported by experimental data. To achieve this, authors altered the original BCC lattice structure, mostly by strengthening them, and used obtained results to provide the aforementioned theoretical approach. The study highlighted the importance of lattice design on the mechanical performance of implants, demonstrating the ability of additive manufacturing to create structures with improved strength and durability needed for biomedical applications. Mascheri et al [43] investigated BCC and BCC-Z reinforced lattices for compressive response, mechanical properties and energy absorption. The study found that BCC-Z lattices with additional vertical supports exhibited significantly higher energy absorption capacity compared to BCC lattices, absorbing ~114% more energy per unit volume before full compression. This result shows the potential of BCC-Z lattices in energy absorbing applications such as collision protection. In addition, the author delivered Gibson-Ashby coefficients for BCC and BCC-Z lattices, which improved predictive models for lattice design and demonstrated the importance of understanding the deformation and energy absorption processes of lattice structures. Additionally, Onal et al. [44] investigated porous Ti6Al4V frameworks for deriving the correlation between mechanical properties and biological response. By altering the diameter of the strut within the BCC unit cell, authors demonstrated the ability to create scaffolds within the framework. This resulted not only in meeting mechanical requirements but also in supporting the cellular activity required for bone tissue engineering. This approach will benefit in development of orthopedic implants that optimize both structural and biological functions to meet the complex demands of bone regeneration. Smith, Guan and Cantwell [45] developed finite element models to predict the compression response of BCC and BCC-Z lattices fabricated using SLM. Authors

managed to demonstrate the feasibility of using finite element analysis to predict the mechanical response of lattice structures through investigating experimental data of collapse modes and stress distributions. The study also showed that modifying unit cell geometry can positively impact on compressive stiffness and yield strength, suggesting ways to optimize the mechanical performance of BCC-based lattice structures.

Cubic cell topologies, known for their potential to create parts with customized mechanical properties, are also a research interest of many scientists. This interest is caused by its topology that closely mimics the hierarchical structure of natural bone. However, some research shows that cubic cell topologies are applicable in other industries as well. For example, research made by Zhou and Liu [46] on the application of 3D printing for catalytic applications using cubic base lattice structures illustrates the versatility of cubic lattices beyond biomedical applications. The study shows how cubic cell topologies can be designed to improve mass and heat transfer properties in catalytic reactors, demonstrating the broad applicability of AM-fabricated cubic lattice structures in a variety of industrial applications. Elsayed et al. [47] showed the influence of strut size on the microstructure and compressive strength of Ti6Al4V porous lattices. Their research has a positive impact on understanding of how AM process parameters influence the final properties of cubic cell topology structures. Authors observed that smaller strut sizes lead to the formation of titanium carbide precipitates and a mixture of metastable phases. These phenomena affect the mechanical integrity of the fabricated lattice structures. Authors concluded that it is important to balance between strut sizes and material composition when optimizing the mechanical properties of cubic cell lattice structures. Tan et al. [48] evaluated the elastic modulus of 316 stainless steel lattice structures printed by binder jetting. The study includes both experimental studies and the development of a numerical model to predict the effective elastic modulus of fabricated lattice specimens. By comparing the computational results of the numerical model with experimental data, the study validates the proposed model. According to authors, this can help to determine design parameters of lattice structures with desired mechanical properties through binder jetting. The obtained results made a significant contribution to the understanding of the mechanical behavior of metal lattice structures produced by binder jetting. A study by Tanlak et al. [49] focused on the numerical prediction of print density ranges for lattice structures in additive manufacturing. Their work provides theoretical boundaries for the relative densities of cubic lattice types and their

derivatives based on machining parameters and powder size. So, this provides an understanding of the interaction between AM process parameters and achievable lattice structure densities. The proposed numerical model provides insight into design optimization for specific applications by predicting printability limits based on key manufacturing constraints. Sallica-Leva, Giardini and Fogagnolo [50] investigated the microstructure and mechanical behavior of porous Ti6Al4V parts fabricated by SLM, focusing on parts with cubic interconnected pores. Authors delivered the information on the role of energy input in determining the microstructure and mechanical properties of printed parts. Higher energy input were associated with parts having a finer martensitic α' microstructure, which resulted in improved mechanical properties at given relative densities, despite resulting in increased porosity due to unintended pore formation. This study shows the importance of controlling energy expenditure during SLM to tailor the mechanical behavior of cubic lattice structures to potential bone replacement applications.

Table 2.2.1: Tabular summary of various investigated lattice structures

Unit cell	Topology	Fabrication method	Features	Preferred applications	Refs.
Auxetic		AM-assisted investment casting, EBM, SLS, SLM.	Negative Poisson coefficient; significantly high energy absorption.	Energy adsorber, sensor, filter, sandwich panel core, scaffolds, light-weight structure, impact protecting apparatus.	[35-39]
Face-centered cubic (FCC)		SLM, EBM.	Symmetrical in X, Y, Z axes; high stiffness; suitable for energy absorption.	Energy adsorber, lightweight structure.	[40]

Body-centered
cubic (BCC)



SLM, EBM, Symmetrical in Lightweight [41, 42,
SLS. XYZ axes; structure, energy 44]
isotropic in X, Y, adsorber, bone
Z, XY, YZ, XZ, implant.
XYZ directions;
eight struts
connected at the
center of the
cube;

BCC with Z
strut (BCC-Z)



SLM, EBM, BCC with four Lightweight [43,45]
SLS. Z-strut structure, energy
reinforcements; adsorber.
isotropic in X, Y,
YZ, XZ
directions;anisotr
opic in other
directions.

Cubic



SLM, EBM, A cubic frame is Bone implant, [46-50]
SLS, BJ, DIW formed by twelve catalytic
struts; stress structure, energy
concentration adsorber.
may take place in
this structure.

2.3. Heat Treatment Processes on AlSi12

Heat treatment can profoundly influence the mechanical characteristics of a material. Consequently, several investigations on heat treatments were conducted to examine the changes

in mechanical properties and energy absorption of components manufactured via SLM. The study done by Siddique et al. [51] examines the impact of annealing on the tribological and corrosion properties of AlSi12 alloys fabricated via SLM, comparing these properties with those of conventionally cast AlSi12. The investigation included sliding and fretting wear tests, alongside weight loss measurements to assess corrosion behavior, revealing that the as-fabricated SLM material exhibited superior wear resistance compared to both cast and annealed SLM samples. This superiority is attributed to the microstructural refinement induced by SLM, which results in a fine Al-rich cellular structure with Si at the cell boundaries, contrasting with the coarse eutectic structure of cast samples. Annealing altered this microstructure, growing the size of Si particles and reducing their density, which correlated with increased wear and corrosion rates. Specifically, the wear mechanism transitioned from abrasive and oxidative for as-fabricated SLM samples to predominantly abrasive with annealing. Corrosion tests in acidic environments showed that corrosion rates accelerated with annealing temperature due to microstructural changes, where the continuous Si network in as-prepared samples, offering some corrosion resistance, broke down into isolated Si particles in annealed samples, increasing susceptibility to acid attack. This study conclusively shows that while SLM fabrication improves the wear resistance and maintains comparable corrosion resistance to casting for AlSi12 alloys, subsequent annealing can detrimentally affect these properties due to microstructural modifications.

Prashant et al. [52] reported the effect of annealing on the wear and corrosion performance of SLM-fabricated AlSi12 alloys, comparing them with cast AlSi12 counterparts. Materials produced by SLM were found to be superior in wear resistance after pristine post-production, which was attributed to a refined microstructure characterized by a fine Al-rich cellular composition with silicon precipitates at the edges of the cells, in stark contrast to the coarse eutectic structure observed in cast samples. However, annealing destroys this favorable microstructure by enlarging the Si particles and decreasing their density, which consequently increases wear and corrosion rates. In particular, the wear mechanisms evolve from abrasive and oxidative in unannealed SLM samples to predominantly abrasive after annealing. Corrosion testing under acidic conditions also shows that annealing increases susceptibility to acid attack by converting a continuous Si network, which initially provides some corrosion resistance, into

isolated Si particles, thereby highlighting the critical impact of post-treatment heat treatment on tribological and corrosion performance. AlSi12 alloys produced by SLM.

Another investigation by Prashanth, Scudino, and Eckert [53] on AlSi12 alloy fabricated SLM and annealed at 573 K revealed its mechanical behavior at elevated temperatures. Annealing led to Si rejection from the Al solid solution, stabilizing the microstructure for tensile testing between 373 K and 473 K. This treatment resulted in a softened material with reduced yield and ultimate tensile strength but improved plasticity. Furthermore, at higher temperatures, the material exhibited increased ductility, attributed to grain coarsening. These findings show the potential of SLM-fabricated AlSi12, especially post-annealing, for automotive applications requiring materials that maintain consistent properties under thermal stress.

Prashanth et al. [54] investigated AlSi12 annealing at temperatures ranging from 473 K to 723 K. The findings show that it led to notable microstructural changes, primarily in the agglomeration and growth of Si particles, affecting the alloy's mechanical properties. Higher annealing temperatures decreased yield strength and tensile strength, however it led to increase in ductility. This findings demonstrate that strength and ductility can be balanced or changed through heat treatment. So, investigation presents the benefits of heat treatment, such as manipulating with AlSi12 mechanical properties by controlling its microstructure.

Li et al. [55] focused on the improvement of eutectic microstructure and mechanical properties of SLM printed AlSi12 by solution heat treatment. This approach produces a unique microstructure characterized by nano-sized spherical silicon particles within a supersaturated aluminum matrix. Solution heat treatment affected the microstructure by separating Si from the Al matrix. This resulted in improved ductility (approximately 25%). This study demonstrates a method for purifying eutectic Al-Si alloys, which will improve mechanical properties without additional modifications in chemical composition.

Ponnusamy et al. [56] studied SLM printed AlSi12 on the effect of heat treatment at 200 °C and 400 °C. Further its effect on dynamic compression response was investigated. Heat treatment resulted in a noticeable decrease in dynamic fluidity and ultimate compressive strength, especially at 400°C, which is explained by softening due to the growth of silicon-rich precipitates. This process caused microstructural changes, which led to a forming of Si agglomerates, thereby weakening the compressive strength of the alloy. Authors reported that the heat-treated samples showed higher strength but greater deformation, indicating increased

ductility. In addition, analysis of the deformation behavior showed an increase in ellipticity as a function of heat treatment temperature and strain rate. This demonstrated the trade-offs among mechanical properties of AlSi12 during the controlled heat treatment. Another paper on the influence of processing parameters, particularly base plate heating and external heat treatment, on tensile properties was investigated by Prashant et al. [57]. According to authors, heating the base plate at temperatures between 473 and 673 K increases ductility. In addition, post processing heat treatment further influenced the mechanical properties, affecting tensile strength and ductility. This paper demonstrates the role of heat treatment in tensile properties of SLM-printed alloys.

Suryawanshi et al. [58] investigated the effects of laser track direction in SLM and heat treatment on tensile, fracture toughness and fatigue properties. The results show that SLM-processed alloys have a unique microstructure that contributes to high strength and improved fracture toughness. Heat treatment further improves these properties. This demonstrates that SLM printed structures combined with appropriate post-processing can significantly improve product's strength and toughness by manipulating microstructure.

Rathod et al. [59] focused on the influence of scanning strategies and heat treatment. Obtained results show that SLM samples have a fine-mesh microstructure that provides superior wear resistance compared to samples achieved casting, primarily due to the continuous silicon mesh. According to authors, heat treatment changes the microstructure, slightly reducing hardness but maintaining improved properties compared to cast samples. They also reported that scanning strategy and surface orientation have affected wear behavior, indicating anisotropy that is influenced by laser track orientation.

2.4. Mechanical properties of lattice structures

The study of the compressive behavior of lattice structures is extensively covered in the literature, primarily because conducting these tests is simpler than tensile testing. Tensile testing of lattice structures is more challenging due to the need for a specialized apparatus to mitigate the risk of stress concentrations, necessitating further investigation as indicated by Carneiro et al. [60]. Lattice structures, when subjected to compression based on their mode of deformation, are

categorized into two types: bending and stretch-dominated. In stretch-dominated lattices, struts undergo axial deformation, making them stronger compared to their bending-dominated counterparts, where deformation is a result of bending, as illustrated in Figure 2.4.1. Figure 2.4.2 also shows the typical stress vs. strain behavior for both types of lattice structures, including regions of elasticity, plasticity, and densification. Unlike the bending-dominated structures, which have stable plastic zones but are weaker, stretch-dominated lattices exhibit variable plastic zones.

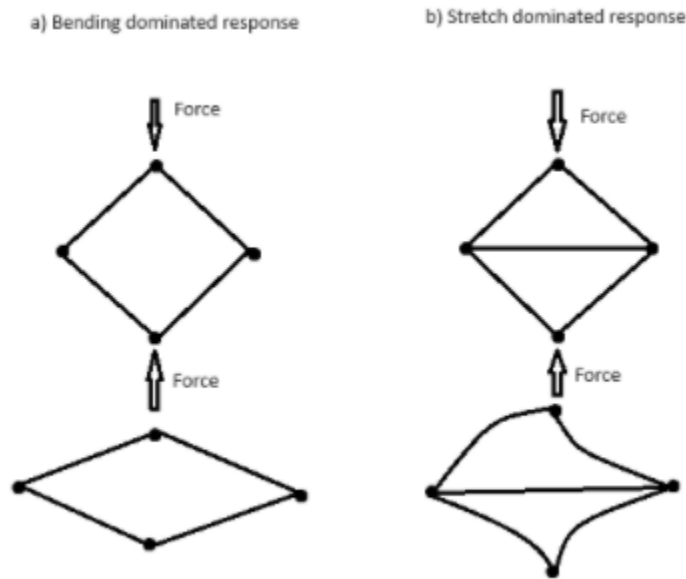


Figure 2.4.1: 2D schematic of bending (a) and stretch dominated (b) deformations

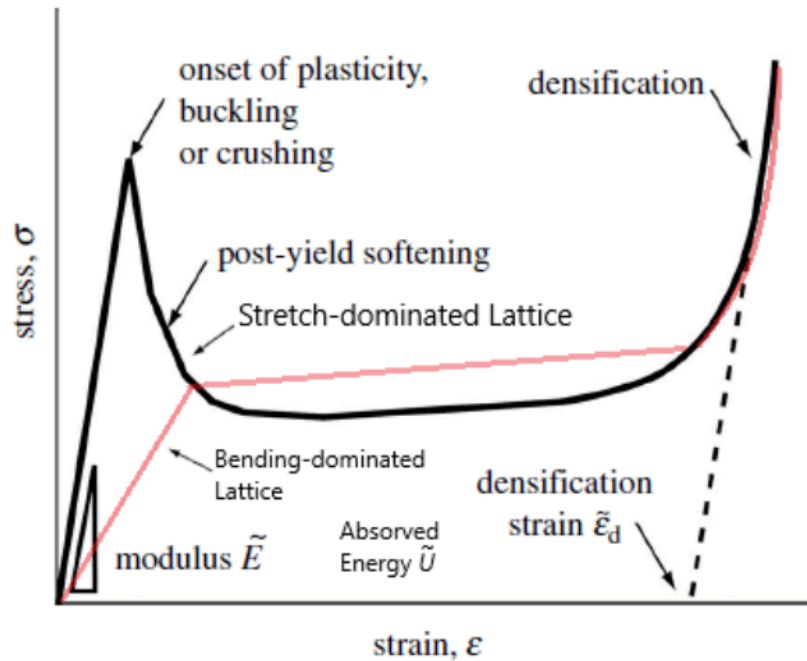


Figure 2.4.2: Standard stress-strain diagrams stretching dominated and bending dominated structures under uniaxial compression [61]

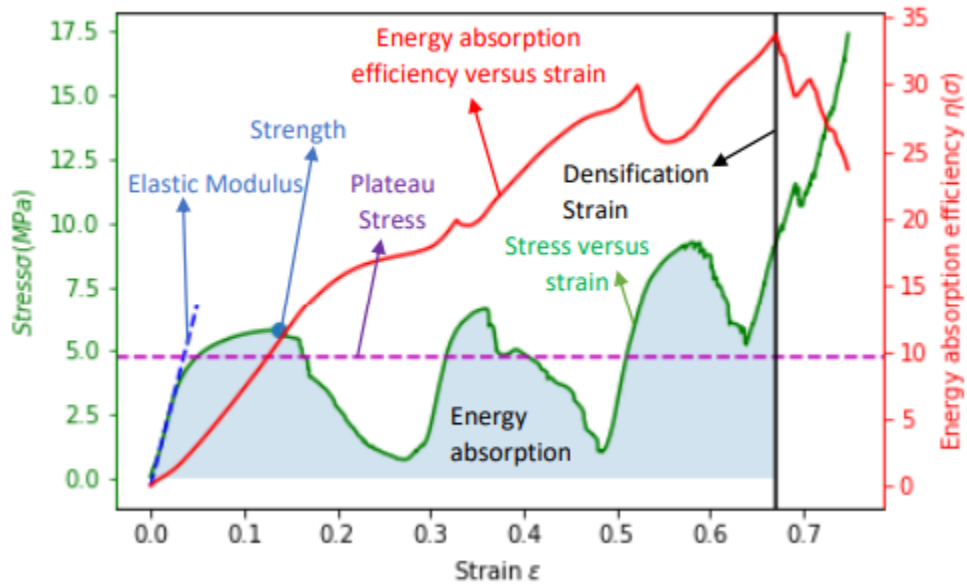


Figure 2.4.3: Schematic of mechanical properties of lattice structures [62]

2.5. Research Gap

The literature review highlights several gaps in the current research on 3D printed lattice structures, including:

- Extensive studies have been conducted on the performance of lattice structures utilizing steel and titanium alloys. While the exploration into Al-Si alloys is thorough, it predominantly centers around AlSi10Mg for the creation of lattice structures. This indicates a notable research void concerning AlSi12.

- Despite the comprehensive examination of various lattice structures, the investigation into how heat treatment influences their energy absorption and mechanical properties remains limited. It has been demonstrated that the material composition can significantly impact the mechanical strength and energy absorption capacity of lattice structures, often more so than their structural topology. Heat treatments, which modify the alloy's microstructure and consequently its mechanical attributes, have been acknowledged in the review for their potential to affect tensile strength, fatigue resistance, and hardness. However, the information available is not exhaustive, suggesting that further studies are needed to elucidate the role of heat treatment in enhancing the mechanical properties of AlSi12.

- Furthermore, there is a noticeable concentration of research on a narrow range of lattice types, with the Kelvin lattice cell emerging as an underexplored area within the industry.

2.6. Motivation, Aim and Objectives

Considering the identified gaps in existing research, this thesis aims to explore the mechanical behavior and energy absorption potential of AlSi12 lattice structures produced via Selective Laser Melting. Our specific goals include:

- Examining the impact of the Kelvin lattice configuration on the performance of AlSi12-based lattice structures.

- Investigating the influence of thermal heat treatments on the mechanical properties and energy absorption efficiency of AlSi12 lattice structures.

- Developing a hybrid lattice design that integrates the Kelvin lattice with a body-centered lattice configuration.

Chapter 3 – Methodology

This segment defines the experimental methodology including the chosen material, design and manufacturing protocols, mechanical investigation, and characterization, along with microscopic examination procedures.

3.1. Powder description

In order to print required specimens AlSi12 powder was purchased from GE Additive. According to the manufacturer, powder size distribution is 20-80 μm . Additional size characterization of powder was performed, results can be seen in figure 3.1. Table 3.1 presents data of powder's size distribution and their respective percentages. Slight deviations in powder composition were detected after performing energy dispersive spectroscopy (EDS) analysis in JEOL JSM-IT200(LA) scanning electron microscope (SEM). The powder particles exhibit a high degree of sphericity with minimal presence of satellite particles, as shown in figures 3.1, 3.2. Notably, internal pores were not detected within the particles. The SEM images, displayed in figures 3.2.2 and 3.2.3, were captured at magnifications of $\times 100$ and $\times 550$ respectively, showcasing the particle morphology.

Table 3.1.1: Tabular summary of powder chemical composition

Component	According to manufacturer (%)	EDS analysis (%)
Si	9.0-11.0	12.72 \pm 0.02
Mg	0.20-0.45	nd
Fe	0-0.55	0.42 \pm 0.00
Mn	0-0.45	0.01 \pm 0.00
Ti	0-0.15	nd
Cu	0-0.10	0.26 \pm 0.01

Zn	0-0.10	0.26±0.01
C	0-0.05	nd
Ni	0-0.05	nd
Pb	0-0.05	nd
Sn	0-0.05	0.02±0.00
Al	Balance	82.05±0.03
O	nd	3.27±0.01

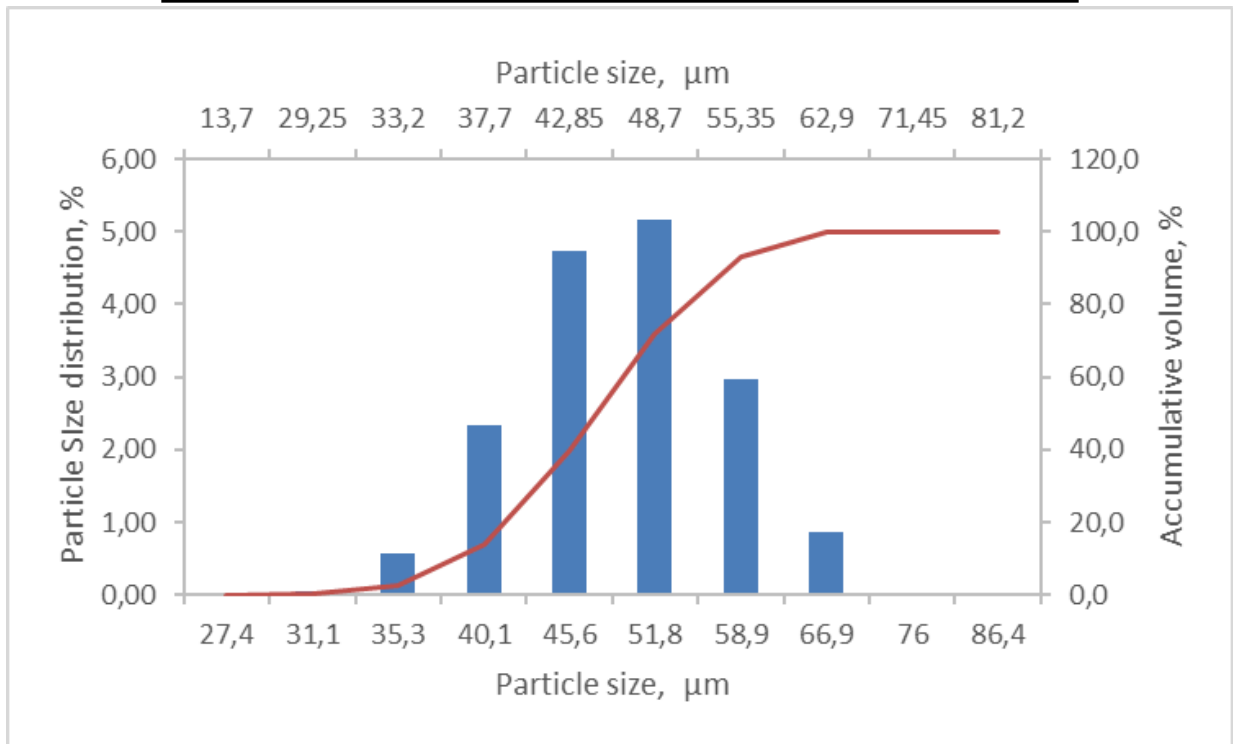


Figure 3.1.1: Size distribution of AlSi12 powder

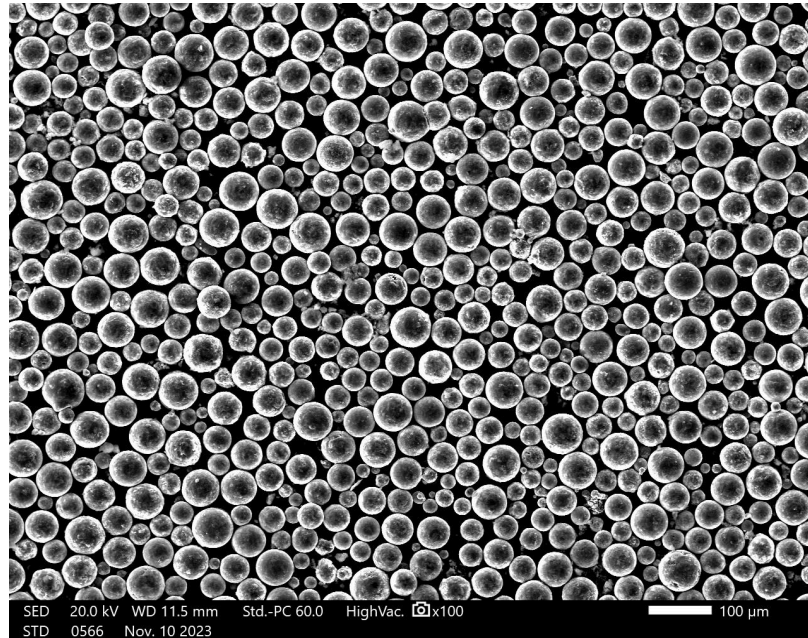


Figure 3.1.2: AISi12 morphology at $\times 100$ magnification

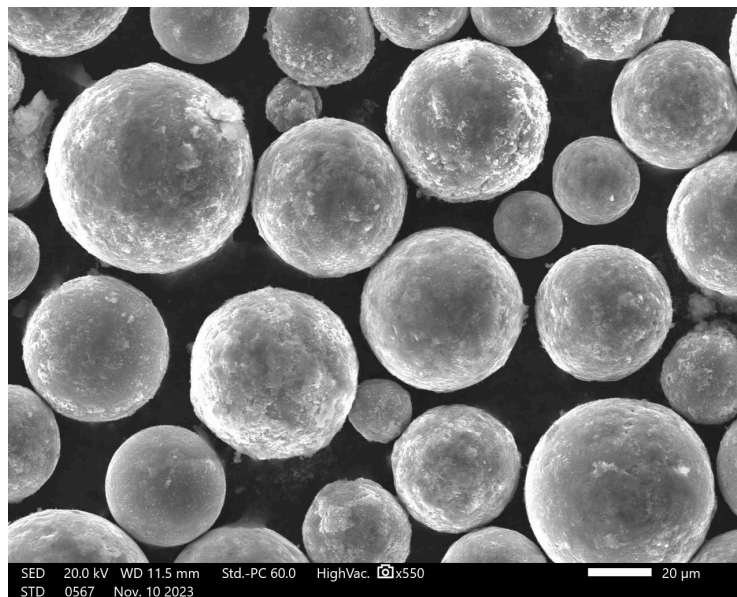


Figure 3.1.3: AISi12 morphology at $\times 550$ magnification

3.2. Lattice structures and tensile specimens

Kelvin lattices (figure 3.2.1-a), characterized by the presence of 14 faces per cell, including 6 squares and 8 hexagons, have been the subject of this investigation. To facilitate the

study, periodic Kelvin lattice specimens composed of $5 \times 5 \times 5$ cells were fabricated via the SLM process utilizing a Renishaw AM400 3D printer. Specimens' characterization is given in table 3.2.1. Since the cross-section area is not distributed uniformly throughout the whole lattice, it was calculated as the average value: volume of lattice was divided by its own height. The infill density is calculated as the ratio of the total volume of the material constituting the lattice's internal structure to the lattice's overall cubic volume. The CAD drawing was done in Solidworks. Additionally, tensile test specimens were prepared to check the bulk properties of a material. The tensile samples feature a gauge length measuring 36 mm and a diameter of 6 mm.

In order to obtain hybrid lattices kelvin lattice was merged with body-centered cubic (BCC) lattice (figure 3.2.1-b) and its slightly altered version. At the end two hybrid lattices were obtained: BCC (figure 3.2.2) and BCC-ALT (figure 3.2.3).

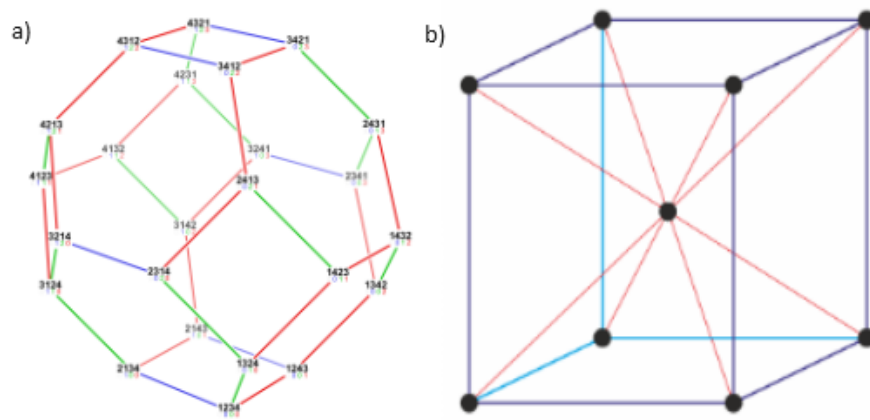


Figure 3.2.1: a) kelvin lattice; b) BCC lattice

Table 3.2.1: Lattice structures' characteristics

	Strut diameter (mm)	Unit cell size (mm)	Average cross-section area (mm ²)	Infill density
15 mm	0.5	3	51.75	0.23
25 mm	1	5	125	0.2
30 mm	1	6	132	0.15
BCC	1	6	272.8	0.3
BCC-ALT	1	6	302.8	0.34

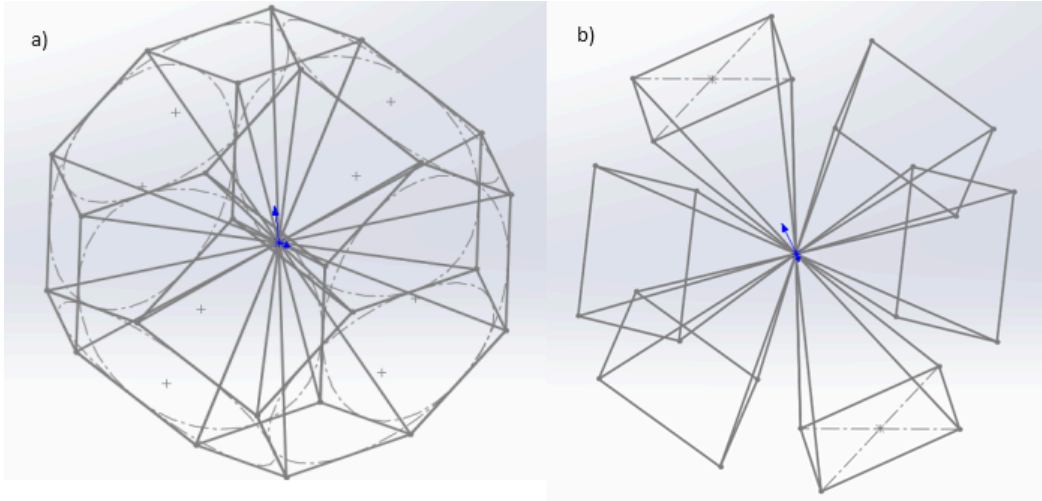


Figure 3.2.2: BCC lattice geometry: a) BCC lattice; b) BCC without kelvin lattice

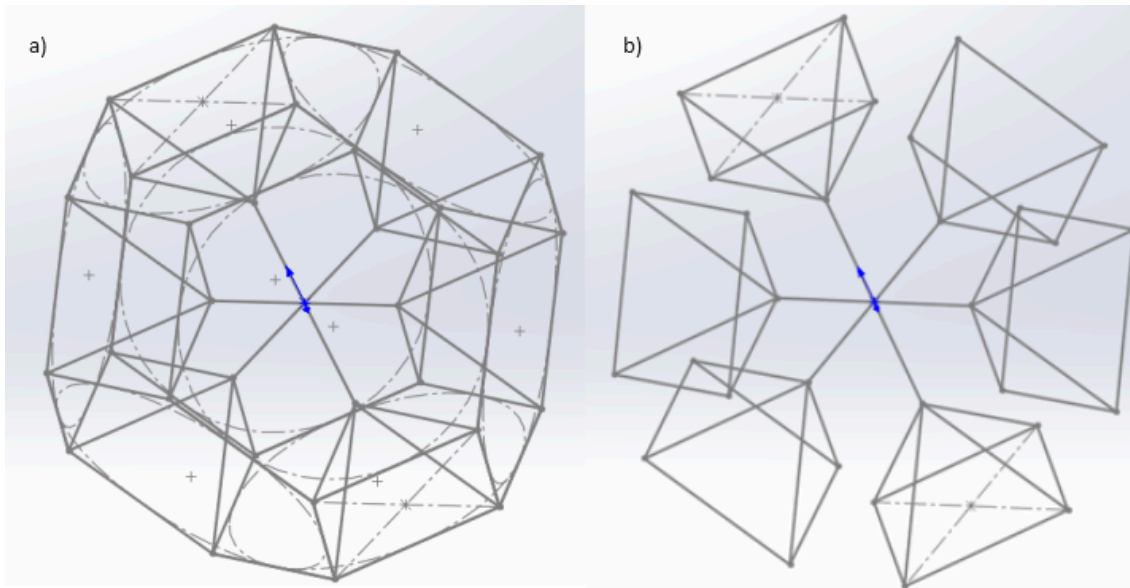


Figure 3.2.3: BCC-ALT lattice geometry: a) BCC- ALT lattice; b) BCC-ALT without kelvin lattice

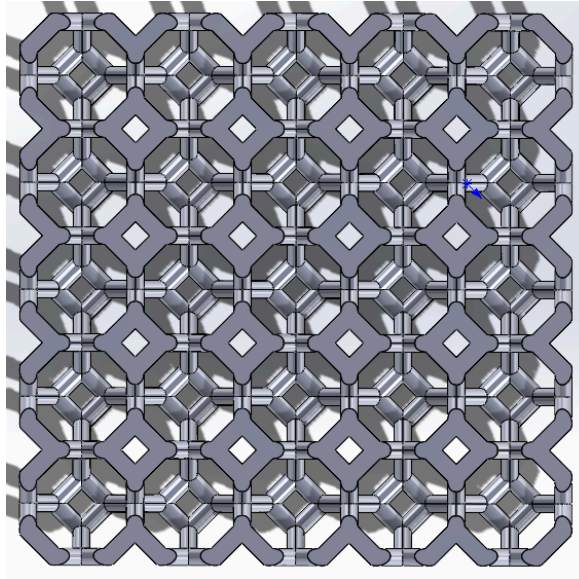


Figure 3.2.4: Cross-sectional view of Kelvin lattice

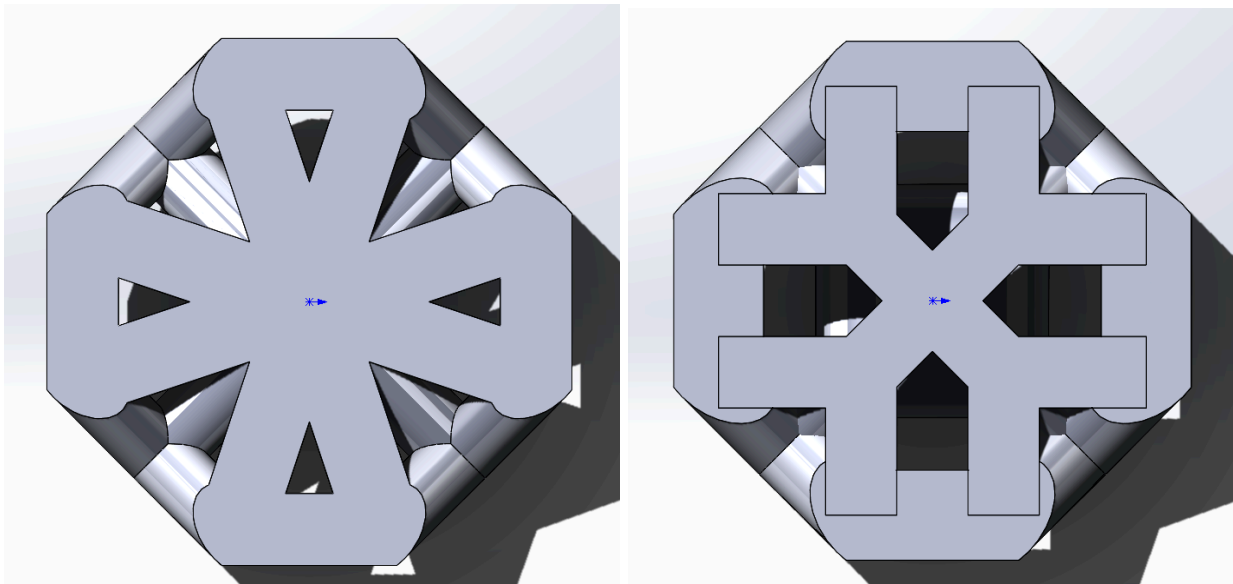


Figure 3.2.5: BCC geometry that was used in hybrid Kelvin lattice: left) Kelvin lattice with BCC; right) Kelvin lattice with altered BCC

3.3. SLM process parameters

The process parameters employed were in adherence to the default recommendations provided by Renishaw, derived from the software library specifically designated for Al-Si alloys. Within this parameter setup, the power ranges between 180 W and 275 W, the scanning speed is

set at 1200 mm/s, and a layer thickness of 30 μm is established. Additionally, the specifics pertaining to point distance and exposure time are detailed in Table 3.3.1.

Table 3.3.1. Printing parameters

Location	Power (W)	Point Distance (μm)	Exposure Time (μs)
Hatch	275	80	40
Core Hatch	180	65	110
Supports	275	80	40

3.4. Specimens characterization

Tensile and compression testing were conducted employing a universal testing machine equipped with a 50 kN load cell, all performed at room temperature.

The tensile assessments were executed according to the ASTM E8M-13a standard guidelines from the American Society for Testing and Materials (2013). The tensile samples comprised a gauge length measuring 36 mm, with a 6 mm diameter. These tests were carried out at a strain rate of 5 mm/min until the occurrence of fracture. Post-test completion, a SEM analysis was employed to scrutinize the fractography of the fractured specimens.

In conducting compression tests on Kelvin lattices, a strain rate of 1 mm/min was applied until it compressed by half of its initial height. Stress-strain curves were derived from load-displacement data. The equations used are as follows:

$$\sigma = \frac{F}{A_0} \quad (1)$$

$$\varepsilon = \frac{\Delta h}{h_0} \quad (2)$$

where σ is stress, F is load, A_0 is cross section area, ε is strain, h is change in height, h_0 is the initial height of the lattice.

To determine energy absorption (ψ), the area under the stress-strain curve for both the elastic and plastic regions was computed, excluding the densification zone, where energy absorption does not occur. Furthermore, the plateau stress (σ_p) was derived from the average stress value in the plastic region. Young's modulus was also calculated in the analysis.

3.5. Heat Treatment

Lattice structures created underwent stress-relief annealing post-manufacture and prior to their removal from the build platform. This annealing process, carried out for two hours at a temperature of 300 °C and followed by cooling at ambient room temperature, aimed to mitigate residual stresses resulting from non-uniform cooling during the SLM process. According to the findings, such heat treatment not only enhances the plasticity of the part but also diminishes its anisotropy. After that part of lattices underwent heat treatment in the temperature range of 480-520 °C, increasing by increments of 20 °C, for a duration of two hours, followed by quenching in water.

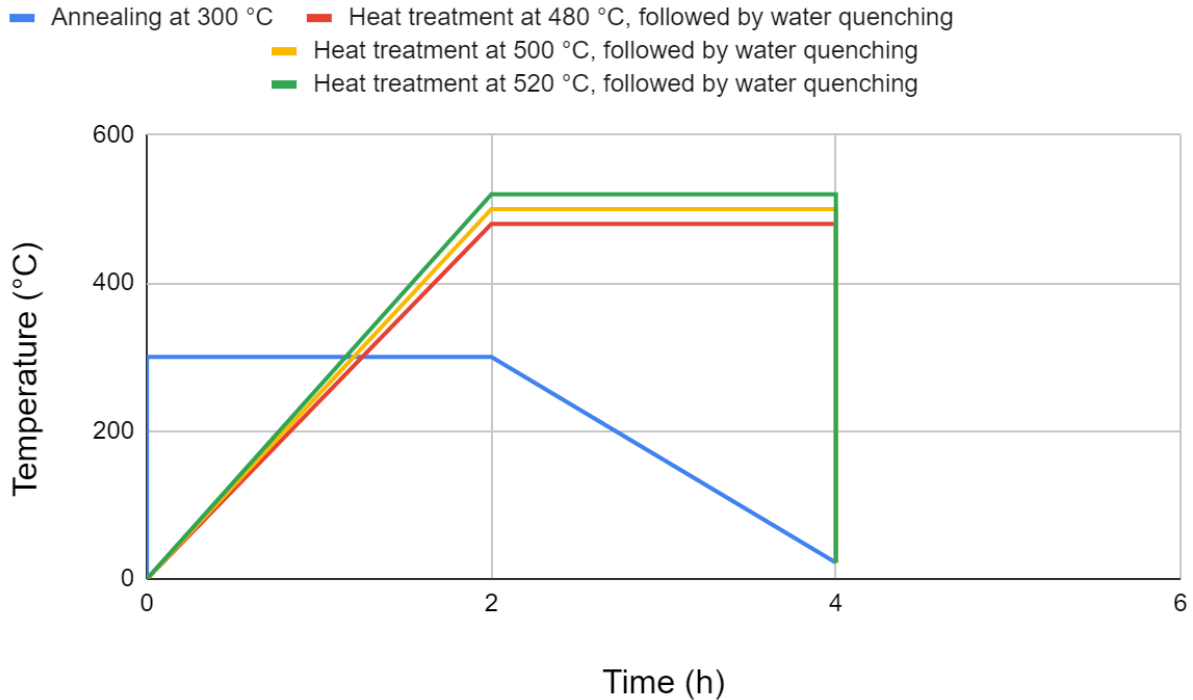


Figure 3.5.1: Heat treatment: temp. vs. time graph

Chapter 4 - Results and Discussion

4.1 Tensile test



Figure 4.1.1: Tensile specimens

The stress-strain responses of the tensile test are shown in figure 4.1.2. Average results of tested samples are 234.45 MPa for yield strength; 335.13 MPa for ultimate tensile strength (UTS); and 86.68 GPa for young's modulus (see figure 4.1.3). These obtained results are similar to those reported by Rashid et al. [63]. They reported that their UTS lies in the range of 260-365 MPa, while yield strength lies between 225-263 MPa. The difference occurs due to different printing parameters, including build orientations (horizontal, vertical, and inclined at 45 degrees). Rashid et al. varied scanning speed within three values: 1000, 1500 and 2000 mm/s. They used a layer thickness of 40 μm and constant power of 285 W.

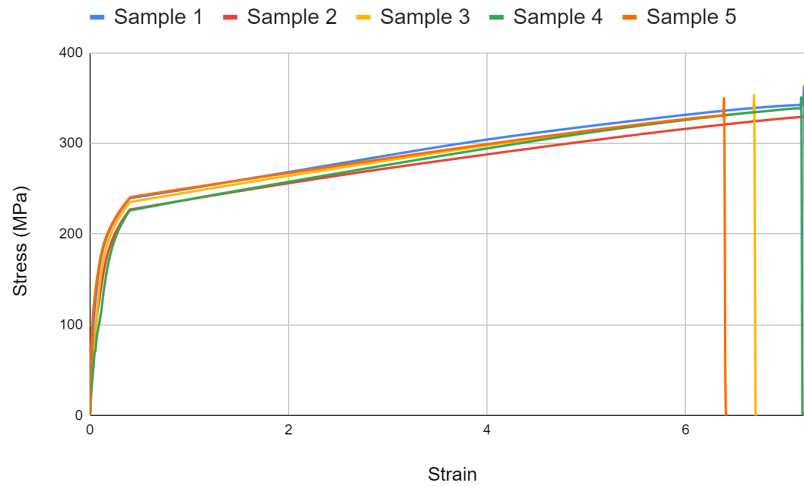


Figure 4.1.2: Stress vs. Strain of tensile test for bulk material

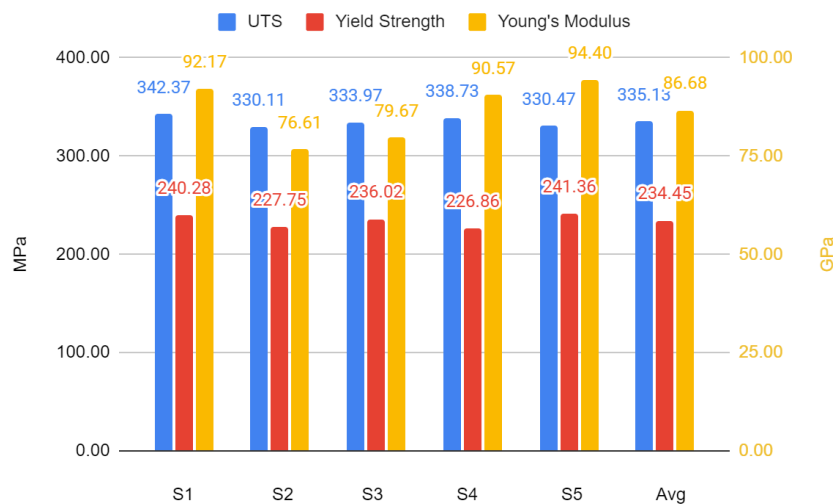


Figure 4.1.3: Mechanical properties of tensile specimens

4.2 Compression test of non heat treated kelvin lattices

Obtained stress-strain responses represented in figure 4.2.1. It gives an average stress-strain curve for 15 mm, 25 mm, and 30 mm kelvin lattices. Additionally, figure 4.2.2 represents yield strength, plateau stress, and young's modulus. Figure 4.2.3 shows energy absorption capacity of given kelvin lattices.

The compression response of kelvin lattices shows that it has stretching dominated topology and delineates into three specific deformation regions, which are elastic, plastic, and

densification zones, refer to figure 2.4.3. Also, within the elastic zone, the stress-strain behavior is linear, displaying a correlation where the degree of linearity corresponds to the lattices' young's modulus. As deformation advances, the curve's gradient diminishes, signifying the lattice's progressive softening. This decrease in slope is indicative of a reduction in the material's stiffness as it undergoes further compression. This sequence unfolds before reaching the peak stress level, subsequent to which there is an abrupt reduction in stress due to the local struts' failure. Following local densification, stress levels rise anew, inducing a recurrent softening-hardening phenomenon within the plastic region, during which the lattice structures actively absorb a substantial proportion of the energy. Upon departing from the plastic region, lattice deformation escalates, instigating inter-layer strut interactions, leading to a swift elevation in stress within the densification zone. This stage marks a point where the lattice loses its capacity to absorb additional energy.

The 15 mm kelvin lattice has lowest values in yield strength, young's modulus, and energy absorption capacity compared to the rest kelvin lattices. The 15 mm lattices have significant drop in stress in the plastic region, but it is not continuous as 30 mm lattice's drop in the plastic region. This resulted in plateau stress value, which is higher for 15 mm kelvin lattice compared to 30 mm lattice. In addition, the 15 mm kelvin lattice reached the densification zone earlier (in terms of strain) compared to the rest of the kelvin lattices. This might be caused due to faster failure of struts in the plastic zone, which resulted in faster collapse of overall lattice, see section 4.5. The quicker strut failure itself also can be tied on its diameter being twice less.

Although its young's modulus is not the highest, the 25 mm kelvin lattice has overall better results than the other two lattices. This can be justified by balanced unit cell size and strut diameter. The stress-strain curve is nearly identical to what 30 mm kelvin lattice has. The difference only is in values. This suggests that smaller unit cell size lattices have superior mechanical properties, given that strut diameters are the same.

As for the 30 mm kelvin lattice, apart from the values, the most significant difference occurs in the plastic region. 30 mm kelvin lattice has a significantly higher drop in stress value. This is probably due to increased strut length. Increased length of strut also resulted in overall stress values.. The reason is due to bending stress, which is higher for longer struts with the same diameter. It can be characterized by $\sigma = My/I$, where σ is the stress, M is the moment, y is the distance from the neutral axis, and I is the moment of inertia.

The energy absorption capacity is highest for the 25 mm kelvin lattice and lowest is for 15 mm lattice. From the results obtained it is assumed that the major role is played by balancing unit cell size and strut diameter, when it comes to mechanical properties.

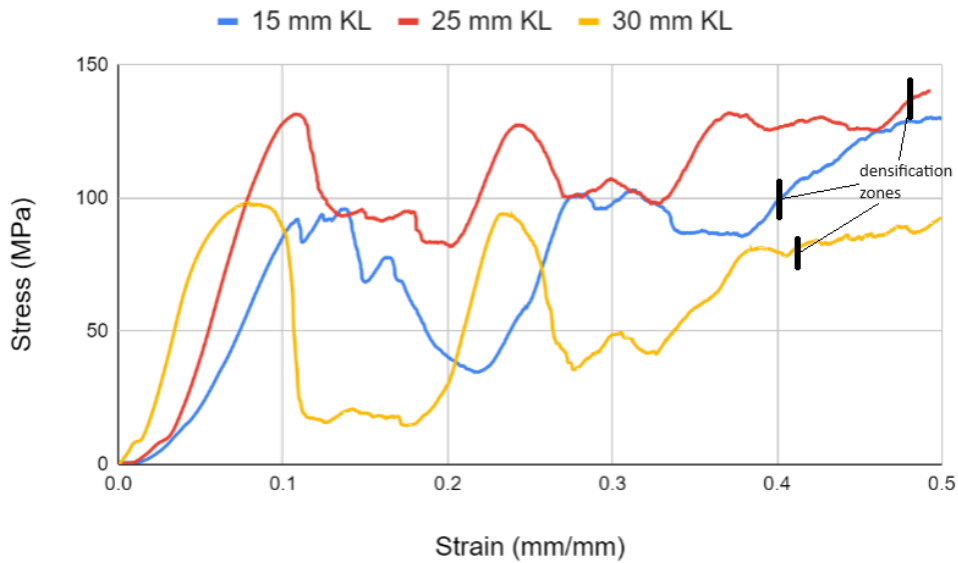


Figure 4.2.1: Compressive stress-strain curve of kelvin lattices

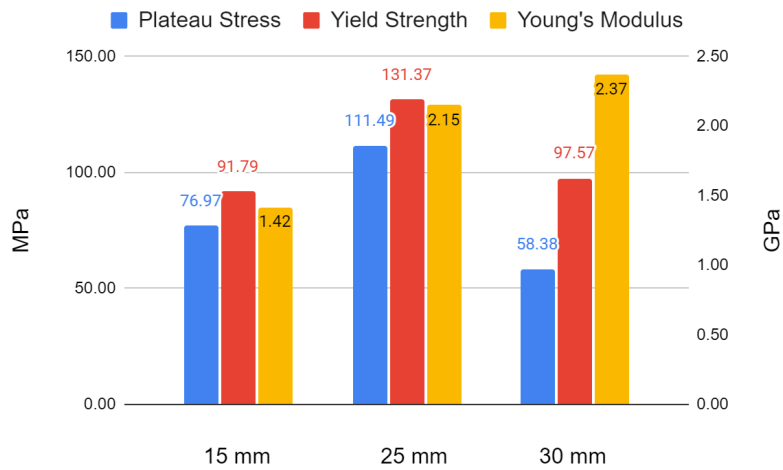


Figure 4.2.2: Compressive mechanical properties of kelvin lattices

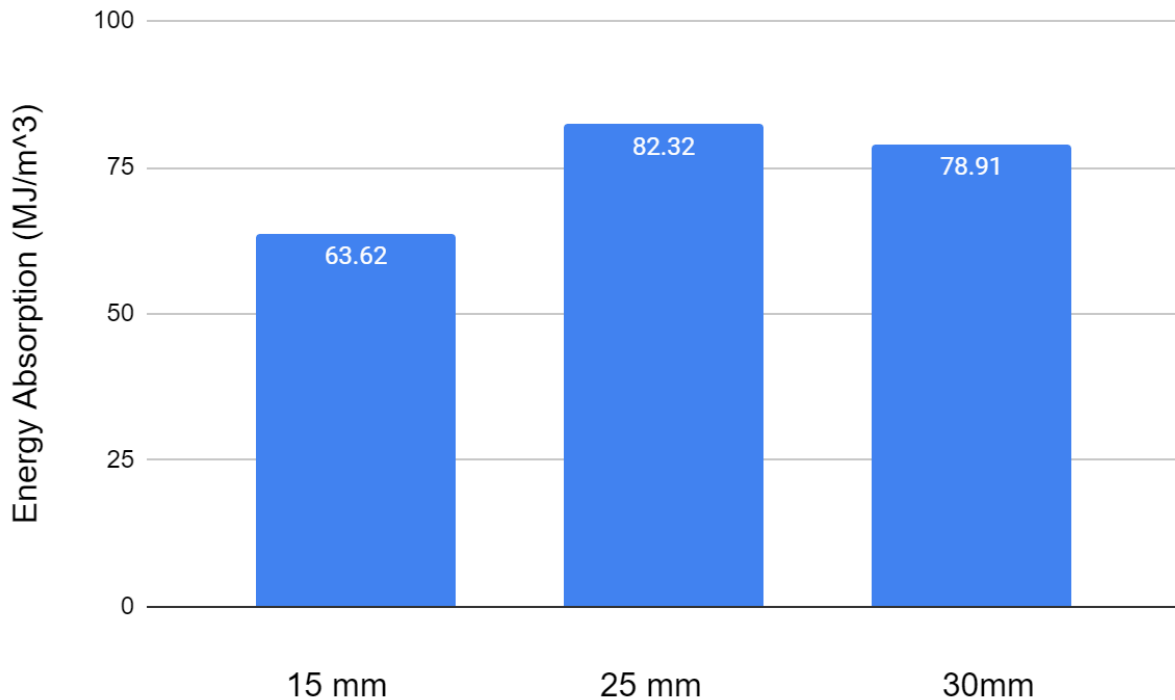


Figure 4.2.3: Energy absorption capacity of kelvin lattices

4.3 Compression test of heat treated kelvin lattices

Figure 4.3.1 shows Stress-strain responses of heat treated Kelvin lattices. Heat treatment increased the ductility of lattice structures, and stretching dominated response changed to bending dominated response. It can be seen that for 25 mm lattices temperature change plays a significant role for 480 °C and 500 °C, however for 500 °C and 520 °C there is only a minor difference. Yield strength also had major drop at 500 °C and 520 °C compared to 480 °C.

The 30 mm kelvin lattice has a similar response, but with lower stress values throughout the graph. The reason behind this is probably due to higher buckling response caused by longer strut length.

All four curves show an initial elastic region where stress increases almost linearly with strain, indicating that the material behaves in an elastic manner. As the strain increases, all four curves exhibit a similar pattern of behavior. As the strain approaches roughly 0.05-0.07 mm/mm, the rate of increase in stress begins to decrease, indicating that the material is starting to yield and transition from elastic deformation to plastic deformation. The curves then continue to rise, though at a reduced rate, showing that the lattice is hardening and can still sustain increased stress.

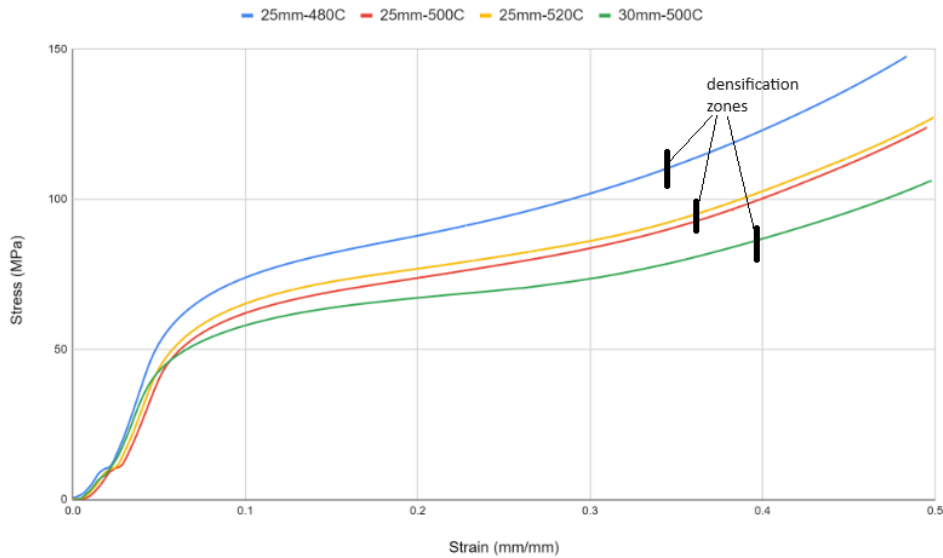


Figure 4.3.1: Compressive stress-strain curve of heat treated kelvin lattices

In terms of numerical values (see figure 4.3.2), 25 mm lattice heat treated at 480 °C showed highest values in yield and plateau strengths, and in young's modulus. Although 25 mm lattices have similar yield strength values, they have notably different values of young's modulus and plateau strength. 30 mm lattice heat treated at 500 °C has the same young's modulus as 25mm lattice heat treated at same temperature, however both yield strength and plateau strength have lower values compared to any heat treated 25 mm kelvin lattices.

As for the energy absorption capacity, 25 mm lattice heat treated at 480 °C has the highest capacity.

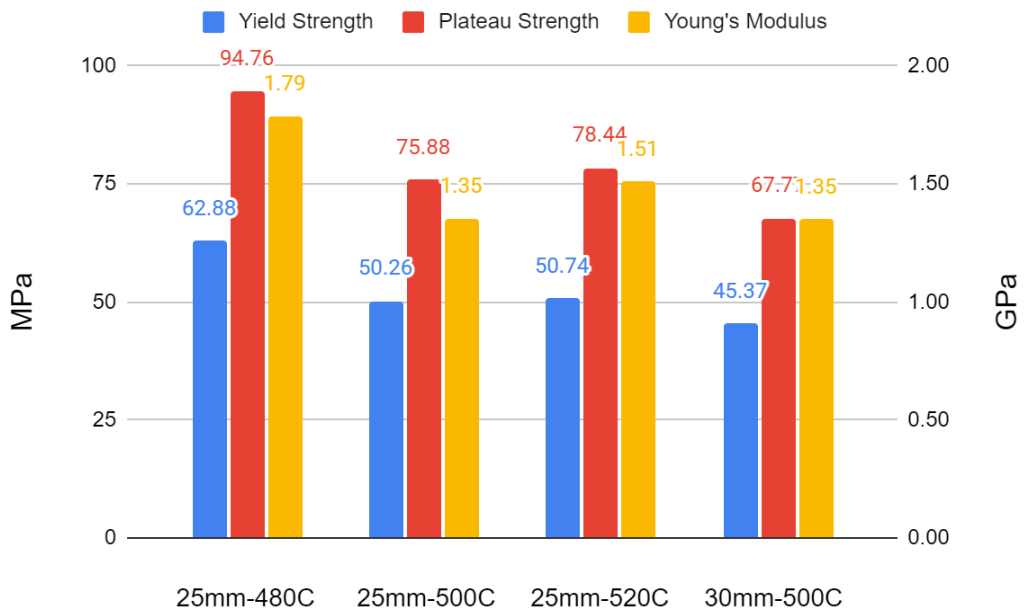


Figure 4.3.2: Compressive mechanical properties of heat treated kelvin lattices

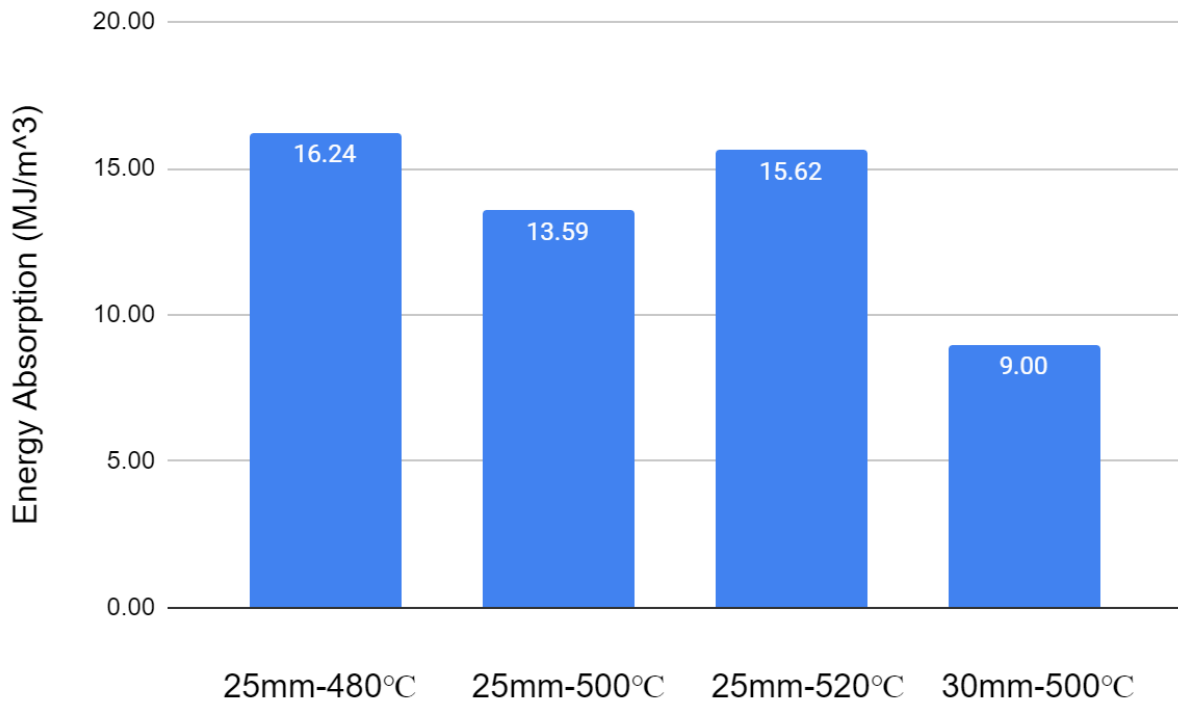


Figure 4.3.3: Energy absorption capacity of heat treated kelvin lattices

4.4 Compression test for hybrid kelvin lattices

Obtained results for non heat treated hybrid kelvin lattices represented in figure 4.4.1. Additionally, figure 4.4.3 represents yield strength, plateau stress, and young's modulus. Figure 4.4.4 shows energy absorption capacity of given hybrid kelvin lattices.

The compression response shows that hybrid kelvin lattices have stretching dominated responses. Within the elastic zone, the stress-strain behavior is similar to kelvin lattices in section 4.2. However, there are almost no fluctuations in the plastic region, except a couple of drops. The BCC lattice reaches the densification zone at ~ 0.46 mm/mm. As for the BCC-ALT, it did not reach the densification zone within the 0.5 mm/mm strain.

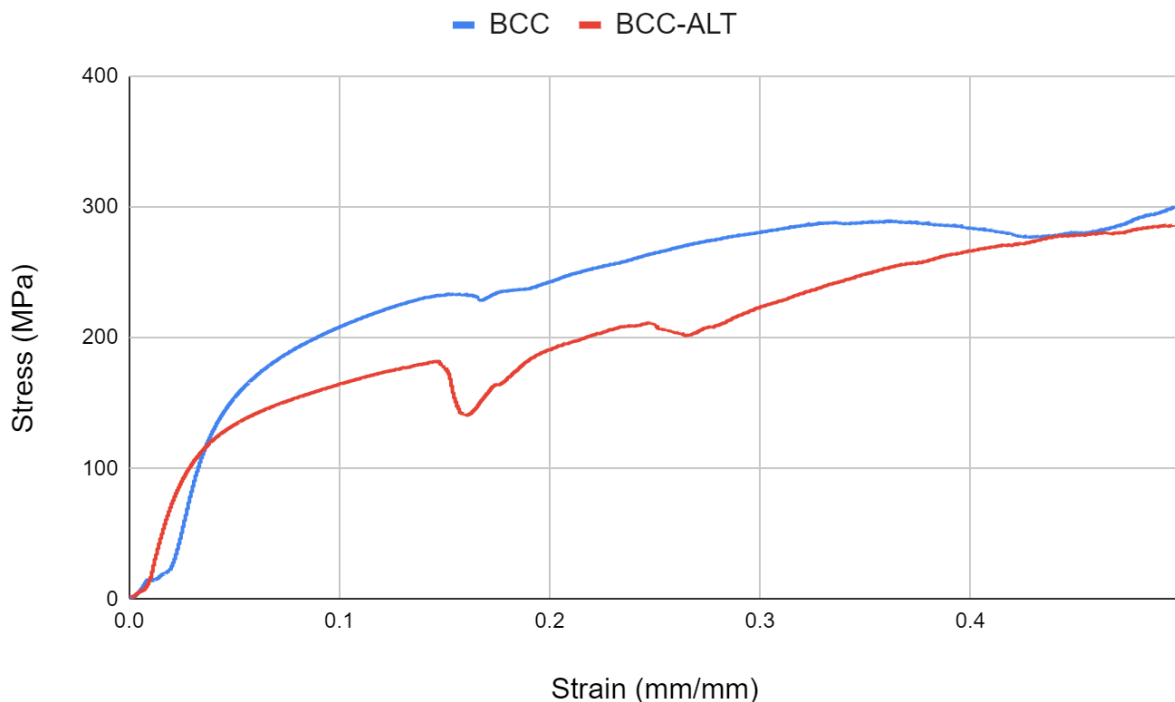


Figure 4.4.1: Compressive stress-strain curve of hybrid kelvin lattices

In figure 4.4.2 hybrid kelvin lattices heat treated at 500°C can be seen. Overall stress-strain response of hybrid lattices shows that kelvin lattice with BCC has greater values compared to kelvin lattice with altered BCC. Similar to kelvin lattices, heat treated hybrid lattices changed their compressive response from stretch dominated to bending dominated

response. However, stress values are increasing at a much higher rate compared to non heat treated samples.

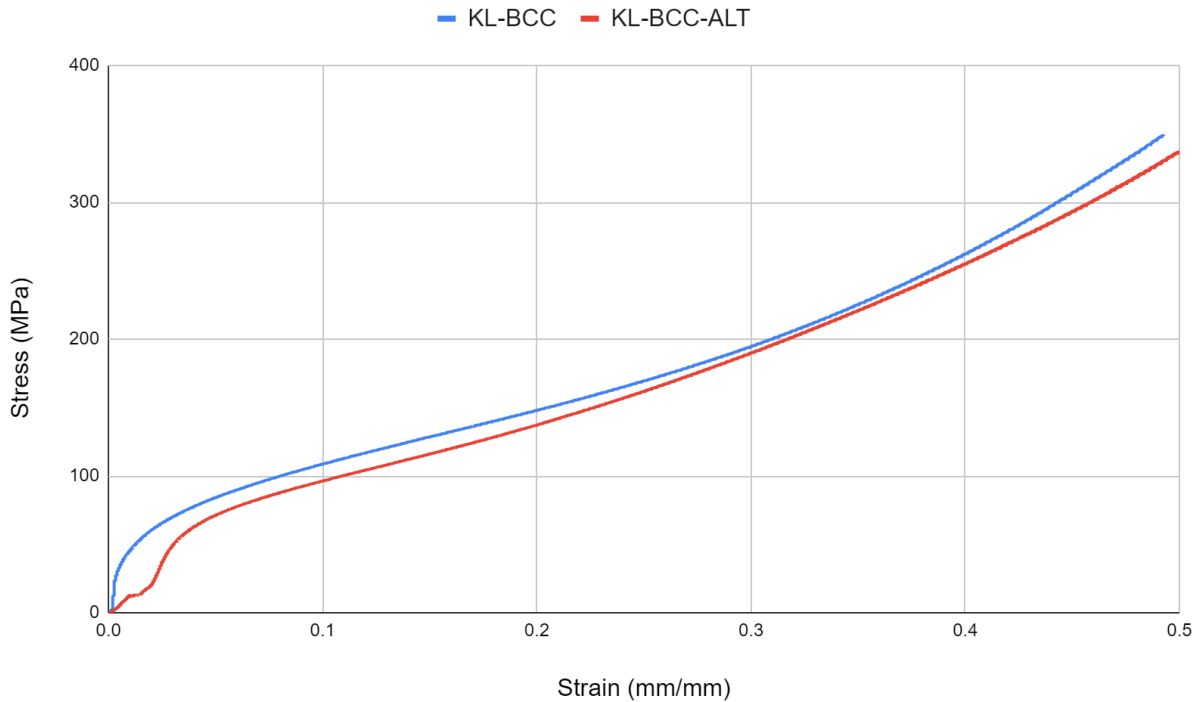


Figure 4.4.2: Compressive stress-strain curve of heat treated hybrid kelvin lattices

In terms of numerical values (figure 4.4.3), both non heat treated and heat treated BCC lattices outperform BCC-ALT lattices when compared to each other. The only exception is that heat treated BCC-ALT has a higher yield point than the BCC lattice. Also, heat treated BCC showed significantly higher young's modulus compared to any other lattice. There is no numerical result of plateau stress for BCC-ALT, since it did not reach the densification zone within 0.5 mm/mm strain.

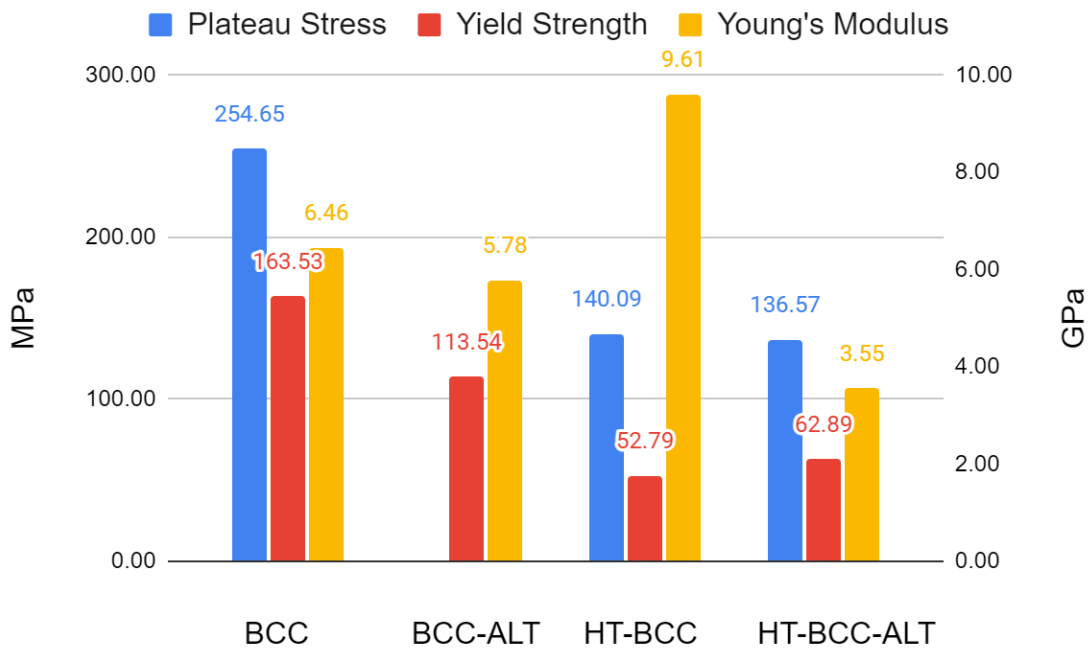


Figure 4.4.3: Compressive mechanical properties of hybrid kelvin lattices

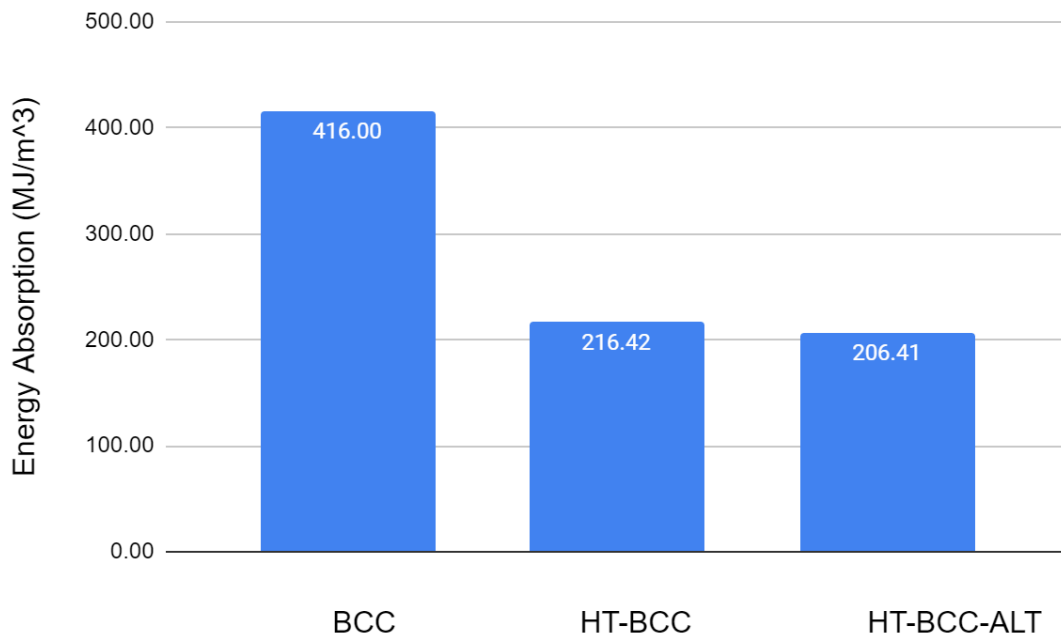


Figure 4.4.4: Energy absorption capacity of hybrid kelvin lattices

4.5 Deformation patterns of non heat treated lattices

As the load intensifies, the vertical struts positioned at the diagonal of Kelvin lattice structures begin to develop hinges as a result of buckling. Owing to the alloy's brittleness, these vertical struts fail, and the load is then transferred to the body-centric struts, which start bending. However, these struts are incapable of enduring significant loads, leading to the fracture of the central node. Consequently, the diagonal loses its capacity to support the load, causing the lattice to split into two distinct segments, resulting in a rapid decline of stress. When the first diagonal fails completely, the second cross diagonal starts to develop due to the similar reason as the first diagonal.

The larger lattice has the same deformation patterns as the smaller one. However, during the failure of the sinister diagonal (Fig. 4.5.2-d) the lower plate of the lattice deformed more than the upper plate. This caused the dexter diagonal to fail in a shifted layer.

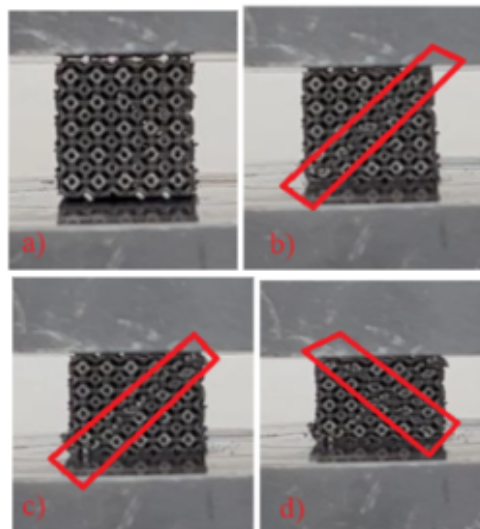


Figure 4.5.1: 15 mm Kelvin lattice deformation patterns. a) Initial state of the lattice; b) sinister diagonal (from upper right to lower left) failure moment; c) sinister diagonal complete failure; d) dexter diagonal (from upper left to lower right) failure moment.

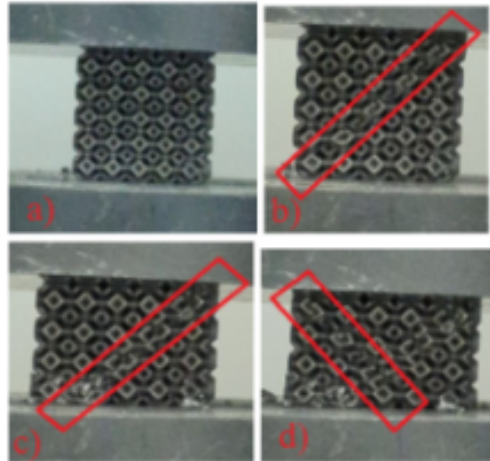


Figure 4.5.2: 25 mm Kelvin lattice deformation patterns. a) Initial state of the lattice; b) sinister diagonal (from upper right to lower left) failure moment; c) sinister diagonal complete failure; d) dexter diagonal (from upper left to lower right) failure moment.

4.6 Deformation patterns heat treated lattices

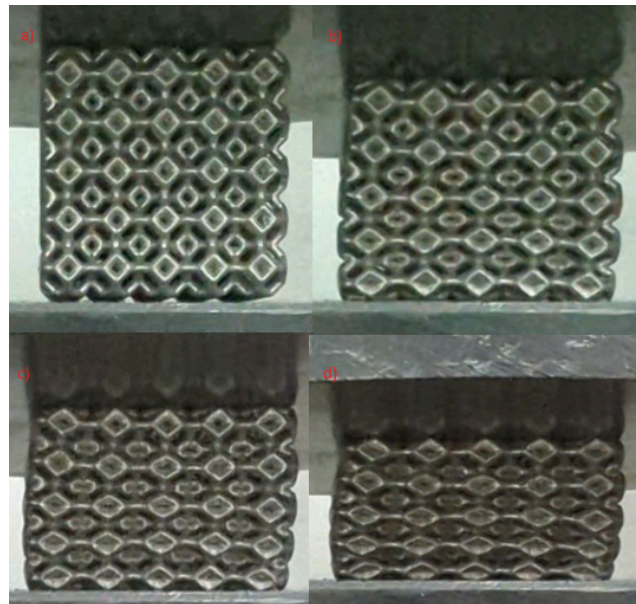


Figure 4.6.1: Deformation pattern of heat treated kelvin lattice. a) Initial state of the lattice; b) yield point; c) plastic region; d) compression at 0.5 mm/mm strain.

As it can be seen from figure 4.6.1, the deformation of heat treated lattices is bending deformation. Struts of heat treated lattices tend to bend, rather than snap as it was observed in non heat treated lattices. This suggests that heat treatment led to an increase in ductility of lattices.

4.7 Tensile specimens fractography

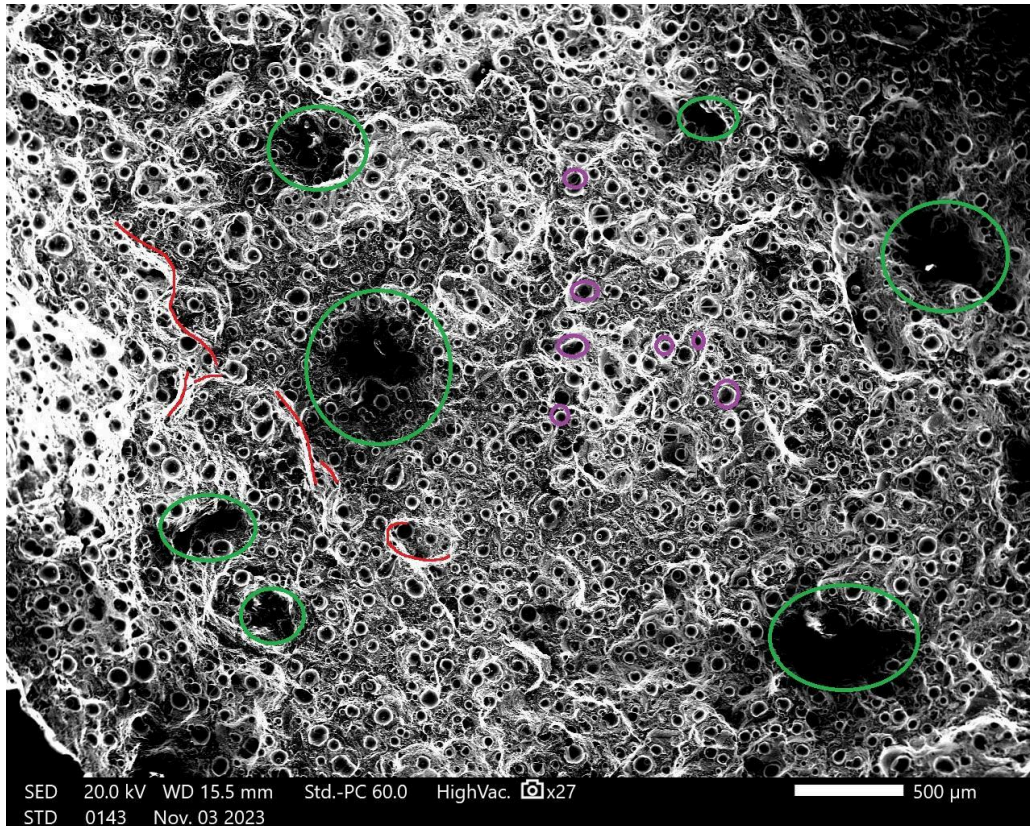


Figure 4.7.1: Tensile specimen fractography

To analyze the fracture surface of tensile specimens, parts were ultrasonically cleaned.

The fracture surface (Figures 4.7.1) reveals numerous small pores with a spherical shape, distributed randomly and averaging 20–80 μm in size. The characteristics of these pores imply that they likely result from either unmelted powder or the presence of small gas bubbles during the SLM. These beads are black spots, highlighted with purple circles. The reason behind this might lie in several places, such as fast scanning speed, low power or both at the same time, improper powder quality or distribution, insufficient inert gas shielding, and suboptimal build

chamber conditions. Additionally, variations in layer thickness and powder particle size can influence the likelihood of porosity formation in the final printed product. The spots indicated by red curves might be indicative of localized plastic deformation or tear ridges. Localized plastic deformation might represent slip bands or localized necking that occurred as the material was stretched. Tear ridges likely develop when cracks intersect individual microvoids positioned ahead of the cracks. Cavities, highlighted by green circles, could indicate ductile dimple rupture, a feature typically found in materials that experienced ductile failure. These dimples are microvoids that coalesce to form the final fracture. Also, green circles might indicate cup-and-cone cavities. They often can be observed in ductile materials undergoing tensile loading. The cup, a depression or concave region resembling a cup, forms due to plastic deformation and necking in the material, resulting from localized stretching and thinning just before fracture. On the other hand, the cone, a raised, conical region surrounding the cup, signifies the area where the final rupture occurred, with the apex of the cone corresponding to the point of initial crack formation. This characteristic cup-and-cone pattern reflects a combination of plastic deformation and localized necking in the material leading up to the ultimate fracture event.

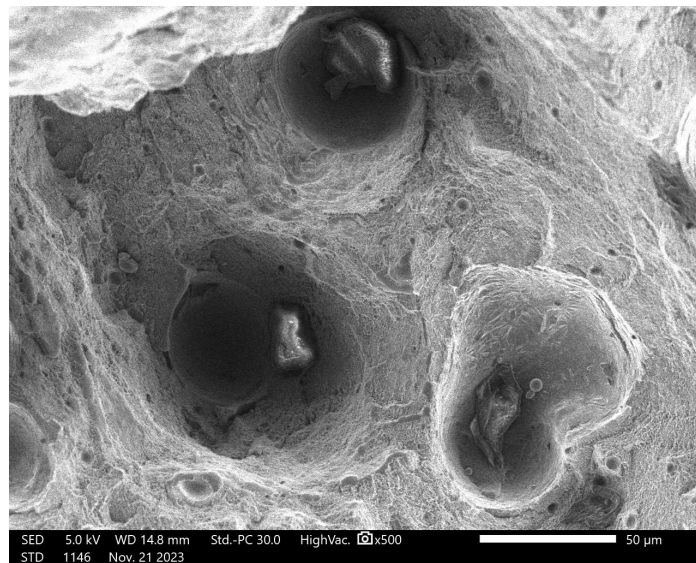


Figure 4.7.2: Tensile specimen fractography

In figures 4.7.2 and 4.7.3 we can observe some particles within dimples. These are unmelted powder particles that were not fully incorporated into the matrix during the printing process. Their presence suggests they could have been initiation sites for the microvoids. The

irregular shapes and the presence of larger voids might indicate lack of fusion. Lack of fusion happens when the laser does not fully melt the powder particles, leading to weak boundaries and gaps between the layers.

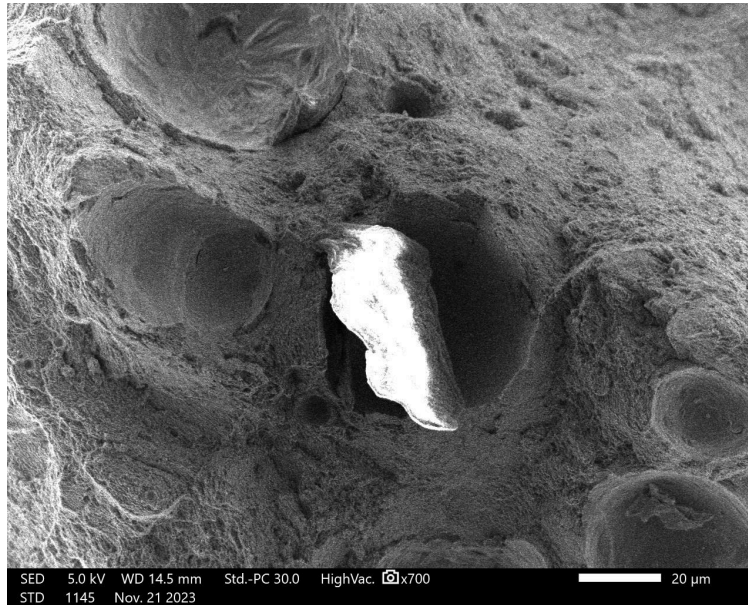


Figure 4.7.3: Tensile specimen fractography

4.8 Microstructure investigation

For microstructure investigation samples with the dimensions of 10×10×1 mm were printed. Samples were polished with silicon carbide sandpaper. Three different grits were used in the following order: 1000, 2400, and 4000. After these samples were additionally polished in diamond suspension polycrystalline (3 µm). The images obtained from SEM are represented in figures 4.8.1 and 4.8.2. They compare the microstructures of AlSi12 alloy in two different conditions: as-built and heat treated at 500°C.

In the figure 4.8.1 the elemental maps for aluminum (Al-K) and silicon (Si-K) show a homogeneous distribution of given elements. The figure 4.8.2 shows noticeable differences. Changes in the microstructure can be observed both in SEM analysis and EDS analysis. The Al-K elemental map still appears fairly uniform, which shows that aluminum's distribution hasn't changed with heat treatment. However, the Si-K map shows considerable clustering, with bright spots indicating a higher concentration of silicon in those areas. This could imply that the heat treatment has caused the silicon to precipitate out of the aluminum matrix, forming silicon-rich

phases. The Si agglomerate resulted in increased ductility, since the Al-matrix is able to deform more freely without the restrictions imposed by the dispersed Si-phase. This explains the difference in compression patterns between as-built and heat treated specimens.

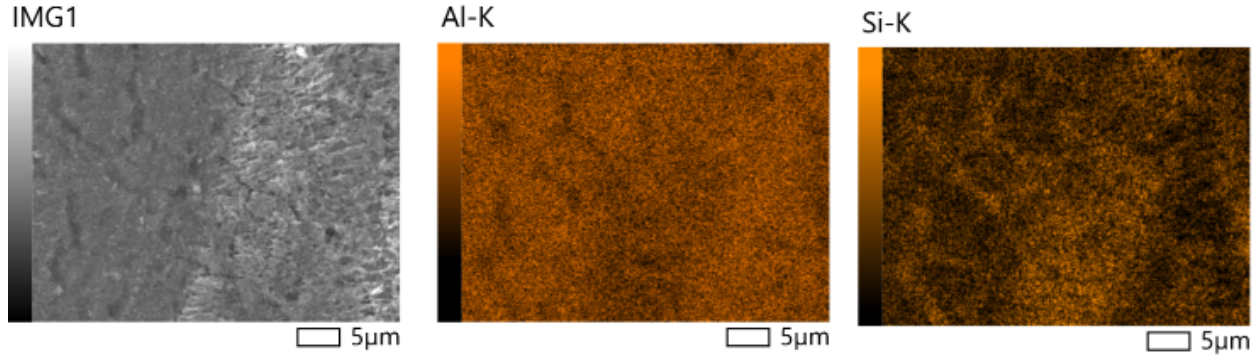


Figure 4.8.1: SEM and EDS images of non heat treated microstructure sample

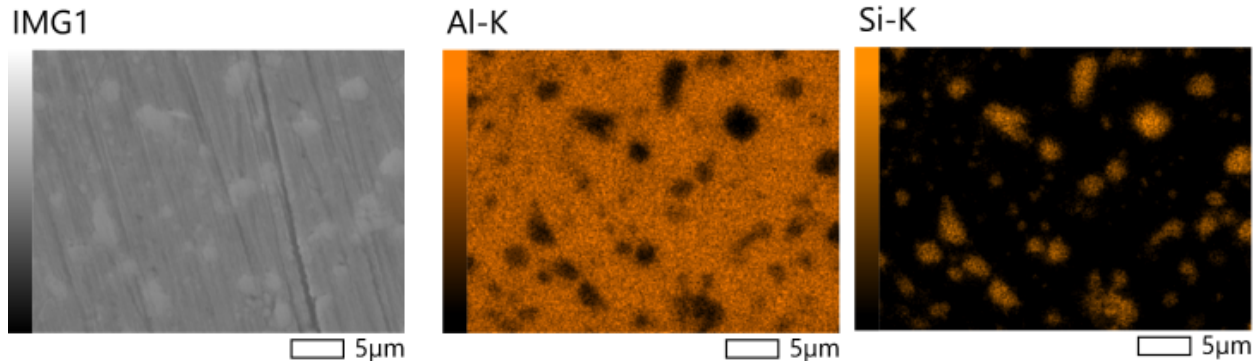


Figure 4.8.2: SEM and EDS images of heat treated microstructure sample

Also, the surface observation of microstructure samples reveals the presence of dimples and cavities, see figures 4.8.3 and 4.8.4. This suggests that samples during the printing indeed faced problems with lack of fusion. Similar dimples were observed in fractography images of tensile specimens in section 4.7.

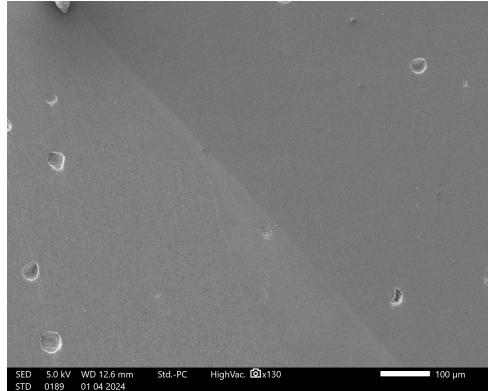


Figure 4.8.3: Microstructure investigation of heat treated sample

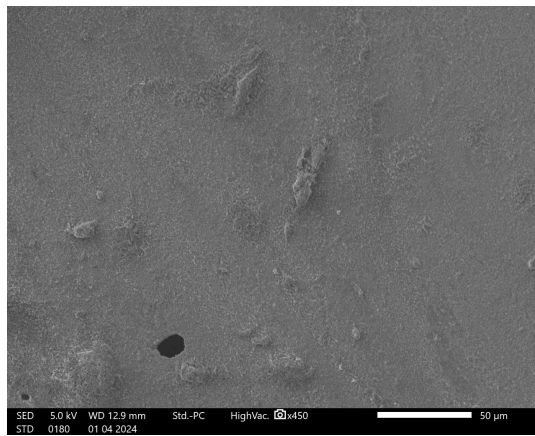


Figure 4.8.4: Microstructure investigation of non heat treated sample

Chapter 5 – Conclusions

Compared with the widely studied AlSi10-Mg alloy, AlSi12 alloy has received less attention from scientists. Moreover, existing studies focus on repeating lattice configurations, including those based on diamond and BCC geometries, thus overlooking a wide range of other lattice structures. Among these overlooked structures is the Kelvin lattice. Hence, this thesis attempted to study AlSi12 Kelvin lattice as well as its integration with bcc lattice structures. Through this study, the mechanical properties and energy absorption capabilities of AlSi12 lattice structures were thoroughly analyzed and presented.

Kelvin lattices with different configurations (strut diameter, unit cell size) were investigated for their mechanical properties and energy absorption capacities. From the results the following conclusion can be made:

- The as-built lattice exhibits superior mechanical characteristics but demonstrates considerable brittleness. Under compression, it develops a shear band, leading to the lattice's total failure. This phenomenon is attributable to the alloy's microstructure, characterized by a fibrous Si network enveloping a fine Al phase.
- Heat treatment affected stress-strain response: the curve changed from stretch to bending dominated response.
- The heat treatment negatively affected energy absorption capacity.
 - Non heat treated lattices can absorb significantly more energy compared to heat treated lattices.
 - Non heat treated kelvin lattice merged with BCC has the highest energy absorption capacity - 416 MJ/m^3
 - The lowest energy absorption capacity of 9 MJ/m^3 belongs to the heat treated 30 mm kelvin lattice.
 - However, heat treatment affected differently on yield point, young's modulus, plateau stress.
- Microstructural analysis showed that heat treatment causes a forming of Si agglomerates, which resulted in increased ductility of lattices.
- Fractography and microstructure investigation revealed that printed samples faced lack of fusion during the SLM printing.

Chapter 6 – Future work

In order to enrich the content of this work and improve results some additional research is recommended:

- In this thesis strut diameter and unit cell sizes were not consecutive. For future work it is recommended to have consistency and evaluate dependence of mechanical properties of a lattice on strut and unit cell size properties more precisely.
- Larger gap in temperature for heat treatment is required to obtain more information on heat treatment effect.
- Tensile test for heat treated specimens is recommended to obtain comparative results.
- Decrease of porosity processes is advised to see by how much mechanical response will change.

References

- [1] W. Gao, Y. Zhang, D. Ramanujan, K. Ramani, Y. Chen, C.B. Williams, C.C.L. Wang, Y.C. Shin, S. Zhang, P.D. Zavattieri, The status, challenges, and future of additive manufacturing in engineering, *Comput. Aided Des.* 69 (2015) 65–89, <https://doi.org/10.1016/j.cad.2015.04.001>.
- [2] B. Nagarajan, Z. Hu, X. Song, W. Zhai, J. Wei, Development of micro selective laser melting: the state of the art and future perspectives, *Engineering* 5 (2019) 702–720, <https://doi.org/10.1016/j.eng.2019.07.002>.
- [3] R. Rahmani, M. Antonov, and K. G. Prashanth, “The Impact Resistance of Highly Densified Metal Alloys Manufactured from Gas-Atomized Pre-Alloyed Powders,” *Coatings*, vol. 11, no. 2, p. 216, Feb. 2021, doi: <https://doi.org/10.3390/coatings11020216>.
- [4] M.F. Ashby, The properties of foams and lattices, *Philos. Trans. R. Soc. A Math. Phys. Eng. Sci.* 364 (2006) 15–30, <https://doi.org/10.1098/rsta.2005.1678>.
- [5] A. Nazir, K.M. Abate, A. Kumar, J.Y. Jeng, A state-of-the-art review on types, design, optimization, and additive manufacturing of cellular structures, *Int. J. Adv. Manuf. Technol.* 104 (2019) 3489–3510, <https://doi.org/10.1007/s00170-019-04085-3>.
- [6] W. Tao, M.C. Leu, Design of lattice structure for additive manufacturing, 2016 *Int. Symp. Flex. Autom.* (2016) 1–3.
- [7] B. Hanks, J. Berthel, M. Frecker, T.W. Simpson, Mechanical properties of additively manufactured metal lattice structures: data review and design interface, *Addit. Manuf.* (2020), 101301, <https://doi.org/10.1016/j.addma.2020.101301>.
- [8] Y. Mass, O. Amir, Topology optimization for additive manufacturing: accounting for overhang limitations using a virtual skeleton, *Addit. Manuf.* 18 (2017) 58–73, <https://doi.org/10.1016/j.addma.2017.08.001>.
- [9] M. Leary, L. Merli, F. Torti, M. Mazur, M. Brandt, Optimal topology for additive manufacture: a method for enabling additive manufacture of support-free optimal structures, *Mater. Des.* 63 (2014) 678–690, <https://doi.org/10.1016/j.matdes.2014.06.015>.
- [10] J.K. Guest, J.H. Prévost, Optimizing multifunctional materials: design of microstructures for maximized stiffness and fluid permeability, *Int. J. Solids Struct.* 43 (2006) 7028–7047, <https://doi.org/10.1016/j.ijsolstr.2006.03.001>.
- [11] A. Ajdari, S. Babaei, A. Vaziri, Mechanical properties and energy absorption of heterogeneous and functionally graded cellular structures, *Procedia Eng.* 10 (2011) 219–223, <https://doi.org/10.1016/j.proeng.2011.04.039>.
- [12] Q.T. Deng, Z.C. Yang, Effect of poisson’s ratio on functionally graded cellular structures, *Mater. Express* 6 (2016) 461–472, <https://doi.org/10.1166/mex.2016.1341>
- [13] L. Barbieri and M. Muzzupappa, “Performance-Driven Engineering Design Approaches Based on Generative Design and Topology Optimization Tools: A Comparative Study,”

Applied Sciences, vol. 12, no. 4, p. 2106, Jan. 2022, doi: <https://doi.org/10.3390/app12042106>.

- [14] R. Vrana, D. Koutny, D. Palousek, and T. Zikmund, “IMPACT RESISTANCE OF LATTICE STRUCTURE MADE BY SELECTIVE LASER MELTING FROM AISi12 ALLOY,” *MM Science Journal*, vol. 2015, no. 04, pp. 852–855, Dec. 2015, doi: https://doi.org/10.17973/mmsj.2015_12_201547.
- [15] L.E. Murr, S.M. Gaytan, F. Medina, H. Lopez, E. Martinez, B.I. Machado, D. H. Hernandez, L. Martinez, M.I. Lopez, R.B. Wicker, J. Bracke, Next-generation biomedical implants using additive manufacturing of complex, cellular and functional mesh arrays, *Philos. Trans. R. Soc. A Math. Phys. Eng. Sci.* 368 (2010) 1999–2032, <https://doi.org/10.1098/rsta.2010.0010>.
- [16] L.E. Murr, K.N. Amato, S.J. Li, Y.X. Tian, X.Y. Cheng, S.M. Gaytan, E. Martinez, P. W. Shindo, F. Medina, R.B. Wicker, Microstructure and mechanical properties of open-cellular biomaterials prototypes for total knee replacement implants fabricated by electron beam melting, *J. Mech. Behav. Biomed. Mater.* 4 (2011) 1396–1411, <https://doi.org/10.1016/j.jmbbm.2011.05.010>.
- [17] S.Lammers, G.Adam, H.J.Schmid, R.Mrozek, R.Oberacker, M.J.Hoffmann, F. Quattrone, B.Ponick, Additive Manufacturing of a lightweight rotor for a permanent magnet synchronous machine, in: *Proceedings of the 2016 6th International Electric Drives Productions Conference*, IEEE, 2016, pp. 41–45. <https://doi.org/10.1109/EDPC.2016.7851312>.
- [18] P.C. Joshi, R.R. Dehoff, C.E. Duty, W.H. Peter, R.D. Ott, L.J. Love, C.A. Blue, Direct digital additive manufacturing technologies: path towards hybrid integration, in: *Proceedings of the 2012 Future Instrumentation International Workshop Proceedings*, IEEE, 2012, pp. 1–4. <https://doi.org/10.1109/FIIW.2012.6378353>.
- [19] M. Helou and S. Kara, “Design, analysis and manufacturing of lattice structures: an overview,” *International Journal of Computer Integrated Manufacturing*, vol. 31, no. 3, pp. 243–261, Dec. 2017, doi: <https://doi.org/10.1080/0951192x.2017.1407456>.
- [20] D. Li, R. Qin, B. Chen, and J. Zhou, “Analysis of mechanical properties of lattice structures with stochastic geometric defects in additive manufacturing,” *Materials Science and Engineering: A*, vol. 822, p. 141666, Aug. 2021, doi: <https://doi.org/10.1016/j.msea.2021.141666>.
- [21] G. Maliaris and E. Sarafis, “Mechanical Behavior of 3D Printed Stochastic Lattice Structures,” *Solid State Phenomena*, vol. 258, pp. 225–228, Dec. 2016, doi: <https://doi.org/10.4028/www.scientific.net/ssp.258.225>.
- [22] Stylianos Kechagias, R. N. Oosterbeek, M. J. Munford, S. Ghouse, and Jonathan R.T. Jeffers, “Controlling the mechanical behaviour of stochastic lattice structures: The key role of nodal connectivity,” *Additive Manufacturing*, vol. 54, pp. 102730–102730, Jun. 2022, doi: <https://doi.org/10.1016/j.addma.2022.102730>.

- [23] W. P. Syam, W. Jianwei, B. Zhao, I. Maskery, W. Elmadih, and R. Leach, “Design and analysis of strut-based lattice structures for vibration isolation,” *Precision Engineering*, vol. 52, pp. 494–506, Apr. 2018, doi: <https://doi.org/10.1016/j.precisioneng.2017.09.010>.
- [24] X. Liu, T. Wada, A. Suzuki, N. Takata, M. Kobashi, and M. Kato, “Understanding and suppressing shear band formation in strut-based lattice structures manufactured by laser powder bed fusion,” *Materials & Design*, vol. 199, p. 109416, Feb. 2021, doi: <https://doi.org/10.1016/j.matdes.2020.109416>.
- [25] F. Caiazzo, V. Alfieri, S. L. Campanelli, and V. Errico, “Additive manufacturing and mechanical testing of functionally-graded steel strut-based lattice structures,” *Journal of Manufacturing Processes*, vol. 83, pp. 717–728, Nov. 2022, doi: <https://doi.org/10.1016/j.jmapro.2022.09.031>.
- [26] X. Guo, X. Zheng, Y. Yang, X. Yang, and Y. Yi, “Mechanical behavior of TPMS-based scaffolds: a comparison between minimal surfaces and their lattice structures,” *SN Applied Sciences*, vol. 1, no. 10, Sep. 2019, doi: <https://doi.org/10.1007/s42452-019-1167-z>.
- [27] N. V. Viet, N. Karathanasopoulos, and W. Zaki, “Mechanical attributes and wave propagation characteristics of TPMS lattice structures,” *Mechanics of Materials*, vol. 172, p. 104363, Sep. 2022, doi: <https://doi.org/10.1016/j.mechmat.2022.104363>.
- [28] S. Catchpole-Smith, R. R. J. Sélo, A. W. Davis, I. A. Ashcroft, C. J. Tuck, and A. Clare, “Thermal conductivity of TPMS lattice structures manufactured via laser powder bed fusion,” *Additive Manufacturing*, vol. 30, p. 100846, Dec. 2019, doi: <https://doi.org/10.1016/j.addma.2019.100846>.
- [29] C. Chatzigeorgiou, B. Piotrowski, Y. Chemisky, P. Laheurte, and F. Meraghni, “Numerical investigation of the effective mechanical properties and local stress distributions of TPMS-based and strut-based lattices for biomedical applications,” *Journal of the Mechanical Behavior of Biomedical Materials*, vol. 126, p. 105025, Feb. 2022, doi: <https://doi.org/10.1016/j.jmbbm.2021.105025>.
- [30] O. Al-Ketan, R. Rowshan, and R. K. Abu Al-Rub, “Topology-mechanical property relationship of 3D printed strut, skeletal, and sheet based periodic metallic cellular materials,” *Additive Manufacturing*, vol. 19, pp. 167–183, Jan. 2018, doi: <https://doi.org/10.1016/j.addma.2017.12.006>.
- [31] F. Günther, M. Wagner, S. Pilz, A. Gebert, and M. Zimmermann, “Design procedure for triply periodic minimal surface based biomimetic scaffolds,” *Journal of the Mechanical Behavior of Biomedical Materials*, vol. 126, pp. 104871–104871, Feb. 2022, doi: <https://doi.org/10.1016/j.jmbbm.2021.104871>.
- [32] N. Novak *et al.*, “Quasi-static and dynamic compressive behaviour of sheet TPMS cellular structures,” *Composite Structures*, vol. 266, p. 113801, Jun. 2021, doi: <https://doi.org/10.1016/j.compstruct.2021.113801>.
- [33] O. Al-Ketan, D.-W. Lee, R. Rowshan, and R. K. Abu Al-Rub, “Functionally graded and multi-morphology sheet TPMS lattices: Design, manufacturing, and mechanical properties,”

- Journal of the Mechanical Behavior of Biomedical Materials*, vol. 102, p. 103520, Feb. 2020, doi: <https://doi.org/10.1016/j.jmbbm.2019.103520>.
- [34] C. Zhang *et al.*, “Mechanical responses of sheet-based gyroid-type triply periodic minimal surface lattice structures fabricated using selective laser melting,” vol. 214, pp. 110407–110407, Feb. 2022, doi: <https://doi.org/10.1016/j.matdes.2022.110407>.
- [35] Y. Xue, X. Wang, W. Wang, X. Zhong, and F. Han, “Compressive property of Al-based auxetic lattice structures fabricated by 3-D printing combined with investment casting,” *Materials Science and Engineering: A*, vol. 722, pp. 255–262, Apr. 2018, doi: <https://doi.org/10.1016/j.msea.2018.02.105>.
- [36] F. Warmuth, F. Osmanlic, L. Adler, M. A. Lodes, and C. Körner, “Fabrication and characterisation of a fully auxetic 3D lattice structure via selective electron beam melting,” *Smart Materials and Structures*, vol. 26, no. 2, p. 025013, Dec. 2016, doi: <https://doi.org/10.1088/1361-665x/26/2/025013>.
- [37] S. Yuan, F. Shen, J. Bai, C. K. Chua, J. Wei, and K. Zhou, “3D soft auxetic lattice structures fabricated by selective laser sintering: TPU powder evaluation and process optimization,” *Materials & Design*, vol. 120, pp. 317–327, Apr. 2017, doi: <https://doi.org/10.1016/j.matdes.2017.01.098>.
- [38] J. Schwerdtfeger, P. Heinl, R. F. Singer, and C. Körner, “Auxetic cellular structures through selective electron-beam melting,” *Physica Status Solidi B-basic Solid State Physics*, vol. 247, no. 2, pp. 269–272, Feb. 2010, doi: <https://doi.org/10.1002/pssb.200945513>.
- [39] I. Eldesouky, O. Harrysson, H. West, and H. Elhofy, “Electron beam melted scaffolds for orthopedic applications,” *Additive Manufacturing*, vol. 17, pp. 169–175, Oct. 2017, doi: <https://doi.org/10.1016/j.addma.2017.08.005>.
- [40] L. Bai, J. Zhang, X. Chen, C. Yi, R. Chen, and Z. Zhang, “Configuration Optimization Design of Ti6Al4V Lattice Structure Formed by SLM,” *Materials*, vol. 11, no. 10, p. 1856, Sep. 2018, doi: <https://doi.org/10.3390/ma11101856>.
- [41] M. Leary *et al.*, “Inconel 625 lattice structures manufactured by selective laser melting (SLM): Mechanical properties, deformation and failure modes,” *Materials & Design*, vol. 157, pp. 179–199, Nov. 2018, doi: <https://doi.org/10.1016/j.matdes.2018.06.010>.
- [42] Q. Feng, Q. Tang, Z. Liu, Y. Liu, and Rossitza Setchi, “An investigation of the mechanical properties of metallic lattice structures fabricated using selective laser melting,” vol. 232, no. 10, pp. 1719–1730, Aug. 2018, doi: <https://doi.org/10.1177/0954405416668924>.
- [43] I. Maskery *et al.*, “An investigation into reinforced and functionally graded lattice structures,” *Journal of Cellular Plastics*, vol. 53, no. 2, pp. 151–165, Jul. 2016, doi: <https://doi.org/10.1177/0021955x16639035>.
- [44] E. Onal, J. Frith, M. Jurg, X. Wu, and A. Molotnikov, “Mechanical Properties and In Vitro Behavior of Additively Manufactured and Functionally Graded Ti6Al4V Porous Scaffolds,” *Metals*, vol. 8, no. 4, p. 200, Mar. 2018, doi: <https://doi.org/10.3390/met8040200>.
- [45] M. Smith, Z. Guan, and W. J. Cantwell, “Finite element modelling of the compressive response of lattice structures manufactured using the selective laser melting technique,”

- International Journal of Mechanical Sciences, vol. 67, pp. 28–41, Feb. 2013, doi: <https://doi.org/10.1016/j.ijmecsci.2012.12.004>.
- [46] X. Zhou and C. Liu, “Three-dimensional Printing for Catalytic Applications: Current Status and Perspectives,” *Advanced Functional Materials*, vol. 27, no. 30, p. 1701134, Jun. 2017, doi: <https://doi.org/10.1002/adfm.201701134>.
- [47] H. Elsayed, N. Novak, M. Vesenjaj, F. Zanini, S. Carmignato, and L. Biasetto, “The effect of strut size on microstructure and compressive strength of porous Ti6Al4V lattices printed via Direct Ink Writing,” *Materials Science and Engineering: A*, vol. 787, p. 139484, Jun. 2020, doi: <https://doi.org/10.1016/j.msea.2020.139484>.
- [48] Y. Tang, Y. Zhou, T. Hoff, M. Garon, and Y. F. Zhao, “Elastic modulus of 316 stainless steel lattice structure fabricated via binder jetting process,” *Materials Science and Technology*, vol. 32, no. 7, pp. 648–656, May 2016, doi: <https://doi.org/10.1179/1743284715y.00000000084>.
- [49] N. Tanlak, D. F. De Lange, and W. Van Paepegem, “Numerical prediction of the printable density range of lattice structures for additive manufacturing,” *Materials & Design*, vol. 133, pp. 549–558, Nov. 2017, doi: <https://doi.org/10.1016/j.matdes.2017.08.007>.
- [50] E. Sallica-Leva, A. L. Jardini, and J. B. Fogagnolo, “Microstructure and mechanical behavior of porous Ti–6Al–4V parts obtained by selective laser melting,” *Journal of the Mechanical Behavior of Biomedical Materials*, vol. 26, pp. 98–108, Oct. 2013, doi: <https://doi.org/10.1016/j.jmbbm.2013.05.011>.
- [51] S. Siddique, M. Imran, E. Wycisk, C. Emmelmann, and F. Walther, “Influence of process-induced microstructure and imperfections on mechanical properties of AlSi12 processed by selective laser melting,” *Journal of Materials Processing Technology*, vol. 221, pp. 205–213, Jul. 2015, doi: <https://doi.org/10.1016/j.jmatprotec.2015.02.023>.
- [52] K. G. Prashanth et al., “Tribological and corrosion properties of Al–12Si produced by selective laser melting,” *Journal of Materials Research*, vol. 29, no. 17, pp. 2044–2054, Jul. 2014, doi: <https://doi.org/10.1557/jmr.2014.133>.
- [53] K. Gokuldoss Prashanth, S. Scudino, and J. Eckert, “Tensile Properties of Al-12Si Fabricated via Selective Laser Melting (SLM) at Different Temperatures,” *Technologies*, vol. 4, no. 4, p. 38, Dec. 2016, doi: <https://doi.org/10.3390/technologies4040038>.
- [54] K. G. Prashanth et al., “Microstructure and mechanical properties of Al–12Si produced by selective laser melting: Effect of heat treatment,” *Materials Science and Engineering: A*, vol. 590, pp. 153–160, Jan. 2014, doi: <https://doi.org/10.1016/j.msea.2013.10.023>.
- [55] X. P. Li et al., “A selective laser melting and solution heat treatment refined Al–12Si alloy with a controllable ultrafine eutectic microstructure and 25% tensile ductility,” *Acta Materialia*, vol. 95, pp. 74–82, Aug. 2015, doi: <https://doi.org/10.1016/j.actamat.2015.05.017>.
- [56] P. Ponnusamy et al., “Dynamic compressive behaviour of selective laser melted AlSi12 alloy: Effect of elevated temperature and heat treatment,” *Additive Manufacturing*, vol. 36, p. 101614, Dec. 2020, doi: <https://doi.org/10.1016/j.addma.2020.101614>.

- [57] K. G. Prashanth, S. Scudino, and J. Eckert, “Defining the tensile properties of Al-12Si parts produced by selective laser melting,” *Acta Materialia*, vol. 126, pp. 25–35, Mar. 2017, doi: <https://doi.org/10.1016/j.actamat.2016.12.044>.
- [58] J. Suryawanshi, K. G. Prashanth, S. Scudino, J. Eckert, O. Prakash, and U. Ramamurty, “Simultaneous enhancements of strength and toughness in an Al-12Si alloy synthesized using selective laser melting,” *Acta Materialia*, vol. 115, pp. 285–294, Aug. 2016, doi: <https://doi.org/10.1016/j.actamat.2016.06.009>.
- [59] H. J. Rathod, T. Nagaraju, K. G. Prashanth, and U. Ramamurty, “Tribological properties of selective laser melted Al 12Si alloy,” *Tribology International*, vol. 137, pp. 94–101, Sep. 2019, doi: <https://doi.org/10.1016/j.triboint.2019.04.038>.
- [60] V. H. Carneiro, S. D. Rawson, H. Puga, J. Meireles, and P. J. Withers, “Additive manufacturing assisted investment casting: A low-cost method to fabricate periodic metallic cellular lattices,” *Additive Manufacturing*, vol. 33, p. 101085, May 2020, doi: <https://doi.org/10.1016/j.addma.2020.101085>.
- [61] D. Farias and Guilherme Ribeiro Begnini, “TOPOLOGY AND LATTICE OPTIMIZATION: DESIGN OF WING-FUSELAGE ATTACHMENT COMPONENT FOR AN AERODESIGN AIRCRAFT,” *XXVII Congresso Nacional de Estudantes de Engenharia Mecânica*, Jan. 2020, doi: <https://doi.org/10.26678/abcm.creem2020.cre2020-0107>.
- [62] Syrlybayev, D. (2023). Experimental and numerical investigation of additive manufactured structures. School of Engineering and Digital Sciences
- [63] R. Rashid et al., “Effect of energy per layer on the anisotropy of selective laser melted AlSi12 aluminium alloy,” *Additive Manufacturing*, vol. 22, pp. 426–439, Aug. 2018, doi: <https://doi.org/10.1016/j.addma.2018.05.040>.

Acknowledgements

I would like to seize this moment to express my deepest gratitude and appreciation to my thesis supervisors, Associate Professors Didier Talamona and Asma Perveen. Their support, guidance, patience, and professionalism were indispensable assets that helped me to withstand this academic challenge. I also extend my sincere thanks to my external examiner, Associate Professor Dichuan Zhang, for granting access to his laboratory equipment.

Furthermore, I want to express my heartfelt gratitude to my research colleagues, Andrey Iankin and Albert Pshennikov, for their assistance with operating laboratory equipment. Special thanks go to Anel Zhumabekova, Shahid Ali, and Clifford Omonini for sharing this journey with me and providing invaluable moral support.

I am deeply thankful to the Ministry of Science and Higher Education of the Republic of Kazakhstan and Nazarbayev University for providing the opportunity to work on Project No. OR07665556, entitled “Additive Manufacturing Systems and Metal Powders for the Kazakhstani Industry.”

Last but not least, I want to extend my utmost appreciation and gratitude to my Mother, whose unwavering support and encouragement have been my pillar throughout. Without her guidance and encouragement, I would not have reached the heights of achievement I have attained.

Appendices

Appendices are not necessarily part of every thesis. Appendices may be used for supplementary illustrative material, original data, computer programs, and other material not necessarily appropriate for inclusion within the body text of the thesis.